TWL1 and TWL2 GT: Fracture Containment

Project: 2200261

March, 2023

Trias Westland GT: Fracture Containment

Authors

[redacted]

Reviewed by

[redacted]

Release authorised by:

[redacted], Manager Subsurface and Engineering

Prepared for

HVC
Baanhoekweg 38
3313 LA Dordrecht
Nederland

Prepared by

PanTerra Geoconsultants B.V.
Weversbaan 1-3
2352 BZ Leiderdorp
The Netherlands
T +31 (0)71 581 35 05
F +31 (0)71 301 08 02
info@panterra.nl

Nederlandse samenvatting

HVC heeft PanTerra verzocht om uit te zoeken of het mogelijk is om in Trias Westland te injecteren onder thermisch geïnduceerde scheurcondities in de Delft formatie, zonder verlies van containment door scheurvorming in de afsluitende laag. Dit is belangrijk om te onderzoeken vanwege de toegestane maximale injectiedruk voor geothermische operaties: 0.135 bar/m voor een uitkoeling tot 40°C, hetgeen met 1 bar verlaagd moet worden per graad uitkoeling boven de 40°C (SodM, 2013). Strikte naleving van deze richtlijn zou de injectiecapaciteit van de Trias Westland-injectoren kunnen beperken.

De twee Trias-Westland doubletten liggen binnen het Westland opsporingsvergunninggebied (**Error! Reference source not found.**). De doubletten bestaan uit de producerende put NLW-GT-02 en de injecterende put NLW-GT-01, en uit de producerende put NLW-GT-03 en de injecterende put NLW-GT-04 In deze studie zijn simulaties gedaan van koud waterinjectie onder matrix condities en onder scheurvormende condities. Simulaties onder matrixcondities zijn gedaan om uit te zoeken of het mogelijk is om het beoogde debiet te bereiken zonder de richtlijnen van SodM te overschrijden. Simulaties onder scheurvormingscondities zijn gedaan voor scenario's waar het niet mogelijk is om te injecteren onder matrixcondities, en geven een indicatie van geïnduceerde scheurgroei in de bovenliggende laag voor verschillende parameters. De simulaties laten de impact van koud water injectie zien gedurende de gehele levensduur (30 jaar) van het veld.

De scheursimulaties zijn uitgevoerd met de methode van Gheissary (1998) en van den Hoek (1999, 2000). De methode is een uitbereiding van de Koning methode (1988) die ook gebruikt wordt door TNO (Veldkamp et al., 2016), en bevat meer gecompliceerde geologie met meerdere reservoirlagen en afsluitende lagen.

De putten zijn geboord in het West Nederland Bekken. Het reservoir dat aangeboord is bestaat uit fluviatiele zandstenen van de Delft member, op een diepte van 2313-2392 m TVD (NLW-GT-01) en 2232-2292 m TVD (NLW-GT-04). De reservoirs zijn heel permeabel (700 mD in NLW-GT-01 and 800 mD in NLW-GT-04). De temperatuur van het reservoir is 87°C in NLW-GT-01 en 85°C in NLW-GT-04. Bovenop het reservoir zit de Rodenrijs kleisteen groep, die bestaat uit schalie en de afsluitende laag vormt voor het reservoir. De hele laag wordt geschat op een dikte van 80-83 m. Het onderste deel van deze laag is minder schalie-rijk en heeft daardoor minder goede afsluitende kwaliteiten, dit deel is aangeduid als de "waste zone".

Uit de simulaties van injectie onder matrixcondities blijkt dat als geïnjecteerd wordt met een temperatuur van 25°C (60-62°C uitkoeling), het maximaal toegestane debiet zonder de SodM-limiet voor injectiedruk te overschrijden ongeveer gelijk is aan 580 m^3/h bij NLW-GT-01 en 480 m^3/h bij NLW-GT-04. Aangezien deze debieten ruimschoots hoger zijn dan de voorgenomen debieten van 430 m^3/h (NLW-GT-01) en 300 m^3/h (NLW-GT-04) is het naar verwachting mogelijk om te injecteren onder matrixcondities in beide putten.

De scheursimulaties (zie tabel hieronder) laten zien dat voor alle gesimuleerde scenario's de scheuren klein zijn (< 10 m), met slechts een paar meter penetratie in de waste zone boven de Delft formatie.

Dit rapport bespreekt ook een strategie over hoe het risico van scheurvorming met eventueel verlies van containment gemanaged kan worden. Als onderdeel van zo'n strategie wordt aanbevolen om routine Hall plot analyses te doen, gebaseerd op dagelijkse injectie-data. Injection Fall-Off (IFO) testen kunnen nodig zijn wanneer analyse van de Hall plot de aanwezigheid van een scheur doet vermoeden, hoewel wordt aanbevolen om bij opstarten van de injector altijd (een) IFO test(en) te doen. Temperatuur logging (warm-back surveys) zijn over het algemeen niet nodig, zolang de combinatie van Hall plot / IFO aangeeft dat de gevormde scheur klein blijft.

Om mogelijke scheurvorming te voorkomen in de afsluitende laag wordt geadviseerd om voor injectie in de Delft een druk gradiënt aan te houden die lager is dan 0.158 bar/m. Dat is gelijk aan de minimum in-situ spanningsgradient voor West-Nederland zoals bepaald door Leak-Off Testen (LOT's). Aangezien de afsluitende laag slechts zeer beperkt wordt afgekoeld is de verwachting dat de in-situ spanning in deze laag nauwelijks zal afnemen ten opzichte van 0.158 bar/m en dat daardoor scheurvorming in deze laag niet zal optreden zolang de injectiedruk lager blijft dan 0.158 bar/m. Dat wordt bevestigd door de verschillende scenario's in dit rapport.

NLW-GT-01

Sensitivity	Scenariobeschrijving	Resultaat na 30 jaar
0	Base case	Scheur met een lengte van 2 m geen penetratie van de "waste zone".
1	Lage permeabiliteit (350 mD)	Scheur met een lengte van 7 m met 4 m penetratie in de "waste zone".
2	Lage in-situ stress gradiënt (0.138 bar/m)	Scheur met een lengte van 9 m met 5 m penetratie in de "waste zone".
3	Hoge in-situ stress gradiënt (0.178 bar/m)	Scheur met een lengte van 1 m geen penetratie van de "waste zone".
4	Een hoog debiet van 550 m^3/h	Scheur met een lengte van 3 m met 1 m penetratie in de "waste zone".
5	Een thermo-elastische constante A_T = 1.5 bar/°C	Scheur met een lengte van 4 m met 2 m penetratie in de "waste zone".

NLW-GT-04

Sensitivity	Scenariobeschrijving	Resultaat na 30 jaar
0	Base case	Scheur met een lengte van 1.2 m geen penetratie van de "waste zone".
1	Lage permeabiliteit (350 mD)	Scheur met een lengte van 4 m met 1 m penetratie in de "waste zone".
2	Lage in-situ stress gradiënt (0.138 bar/m)	Scheur met een lengte van 5 m met 2 m penetratie in de "waste zone".
3	Hoge in-situ stress gradiënt (0.178 bar/m)	Scheur met een lengte van 0.8 m geen penetratie van de "waste zone".
4	Een hoog debiet van 400 m^3/h	Scheur met een lengte van 1.4 m geen penetratie van de "waste zone".
5	Een thermo-elastische constante A_T = 1.5 bar/°C	Scheur met een lengte van 3 m geen penetratie van de "waste zone".

Contents

1 Introduction

1.1 General

HVC requested PanTerra to investigate whether it would be possible to inject under induced (thermal) fracturing conditions in Trias Westland. The aim is to inject into the Delft formation, without loss of containment by fracturing into the overlying cap rocks and avoiding possible injection water and/or shallow gas leakage towards ground water. The current maximum allowable matrix injection pressure for geothermal operations *without thermal fracturing* is 0.135 bar/m. This bottom hole pressure corresponding to 0.135 bar/m is allowed for injection temperatures up to 40°C below reservoir temperature. Bottom hole injection pressure has to be lowered by 1 bar per degree beyond 40°C (SodM, 2013). Adherence to this guideline may limit injection capacity of the Trias Westland injectors.

The Trias-Westland doublets, owned by HVC, are situated in the municipality of Westland in the province Zuid-Holland. The doublets, consisting of producer NLW-GT-02 and injector NLW-GT-01 (doublet 1), and of producer NLW-GT-03 and injector NLW-GT-04 (doublet 2) are located within the Westland geothermal exploration concession (Figure 1-1 Top reservoir structural depth map with the subsurface location of the wells (white squares) with reference to the Trias Westland geothermal licences

). The target reservoirs are the fluvial sands of the Delft Sandstone Member, which is the main target of other doublets in this region.

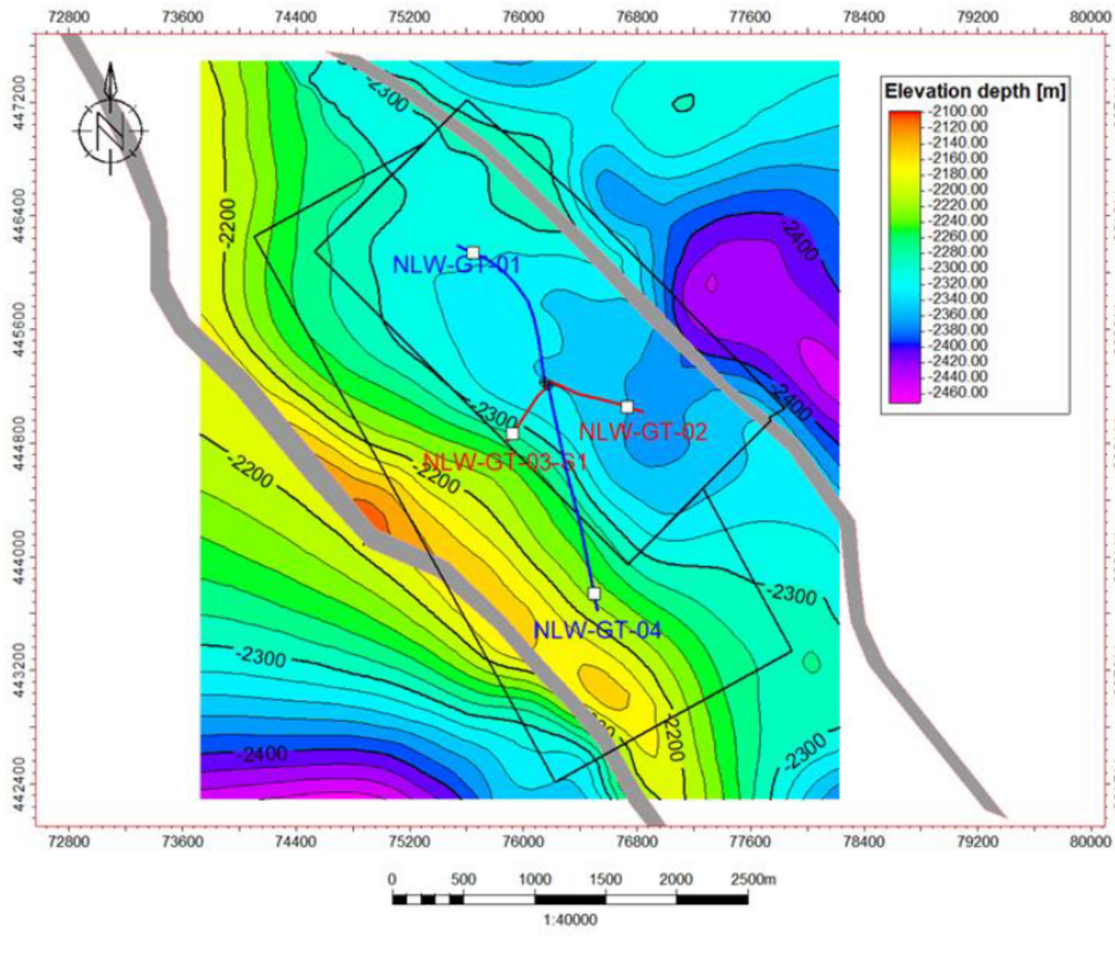

Figure 1-1 Top reservoir structural depth map with the subsurface location of the wells (white squares) with reference to the Trias Westland geothermal licences

In the current study, simulations of cold water injection under both matrix and fracturing conditions have been carried out. Simulations of injection under matrix conditions have been carried out to estimate whether (to which extent) it is possible to achieve target injection rate whilst adhering to the SodM guideline. In addition, simulations under induced fracturing conditions have been carried out to estimate the degree of induced fracture growth into the overlying caprock for a range of uncertain parameters. Both matrix and fracture simulations cover the impact of cold water injection over the entire field life period of 30 years.

Fracture simulations have been performed using the methodology of Gheissary (1998) and van den Hoek (1999, 2000). This is an extension of the Koning method (Koning, 1988) that is also used by TNO (Veldkamp et al., 2016), including more complicated geologies with multiple layers of reservoir and cap rock.

1.2 Objectives

Within the SodM protocol for maximum injection pressures (SodM, 2013), the intention of limiting the pressure is to safeguard the environment of the injection well. The principle of 'containment' and 'confinement' describes the limits of the sphere of influence of the doublet. In the licensed volume (the container) it is acceptable that on a limited scale (by temperature effects) fractures are induced to layers other than the formation in which injected. However, it must be demonstrated that the integrity of the overlying layers that have been defined as seals (confinement) is not affected. Also the induced fractures, and thus the flow of injected cold water, have to remain within the areal limits of the permit.

More recently a "toezichtsignaal Integriteit van het geothermisch reservoir en de afsluitende lagen" (SodM, 2020) was published by SodM in which it was explicitly stated that induced fractures shall not at all penetrate from the reservoir into adjacent cap- or baserock. However, it is noted that deviations from the methodology can be allowed if operations can be performed safely.

The current work is aimed at investigating whether in the presence of induced (thermal) fractures, the injected water in Trias Westland is still contained as mentioned in the SodM protocol (2013) and the "toezichtsignaal". This applies to injection into the Delft formation.

In summary, the objective of the current study is to prevent the risk of unacceptable/ uncontrolled induced fracture growth into the cap rock, by establishing responsible limits for injection parameters in relation cap rock and reservoir.

2 Injection under matrix conditions

For Trias Westland, the reservoir temperature is 85°-87° C at the target injection depths. Using the SodM criteria as mentioned above, the maximum allowable injection rate and tubing head pressure (THP) that avoids thermal fracturing are given in Figure 2-1 and 2-2.

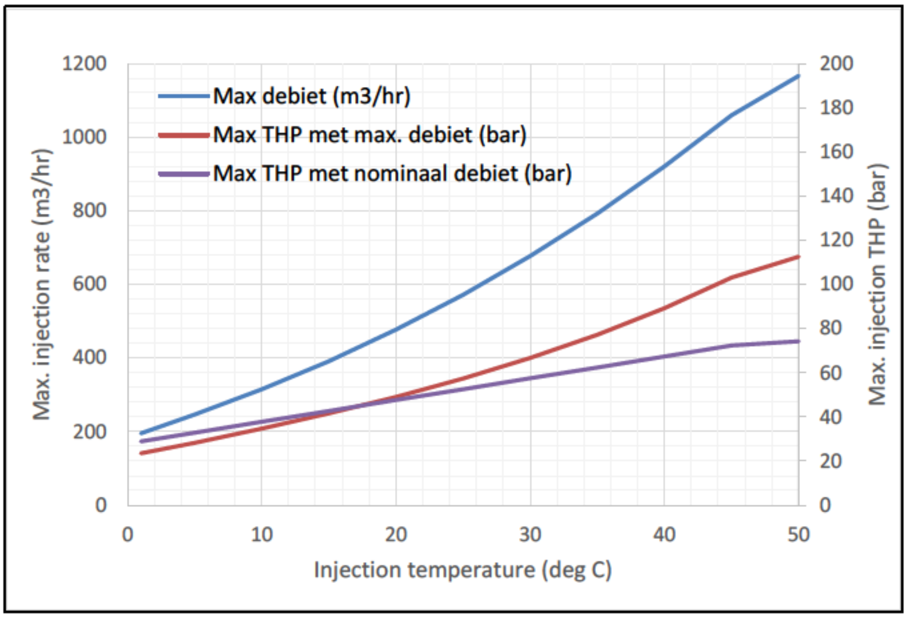

Figure 2-1: Maximum allowable injection rate and THP *without allowing thermal fracturing* for NLW-GT-01 Delft formation, as a function of injection temperature.

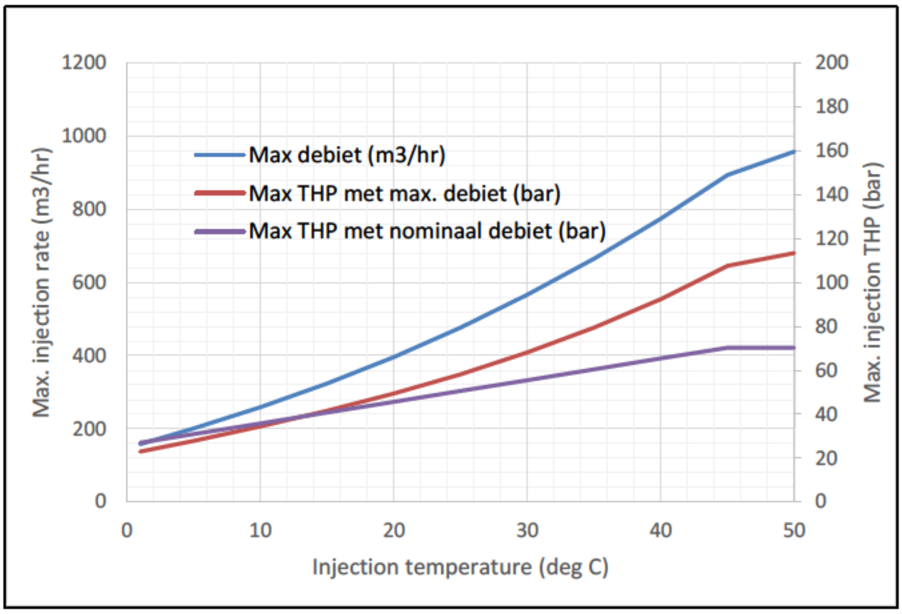

Figure 2-2: Maximum allowable injection rate and THP *without allowing thermal fracturing* for NLW-GT-04 Delft formation, as a function of injection temperature.

The figure shows that with an injection temperature of 25°C, the maximum allowable injection rate is around 580 m^3/hr for NLW-GT-01 and 480 m^3/hr for NLW-GT-04. These values are amply above the intended instantaneous (and not yearly average) target injection rates of 430 m^3/hr and 300 m^3/hr, respectively, for both wells. Therefore, it is expected that it is possible to inject under matrix conditions.

3 Description of mechanisms that can affect the integrity of the seal

3.1 Mechanisms and risks

The risk of affecting seal integrity can be subdivided into two risks:

1. The risk of creating a sizeable induced fracture in the reservoir rock (Delft)

2. Once a sizeable fracture has been created, the risk of upward fracture growth into the seal and possibly beyond, with the ultimate consequence of leaking water and (shallow) gas getting into contact with the ground water.

Figure 3-1 and Figure 3-2 show bowtie diagrams for both of these risks. Please note that both diagrams are linked.

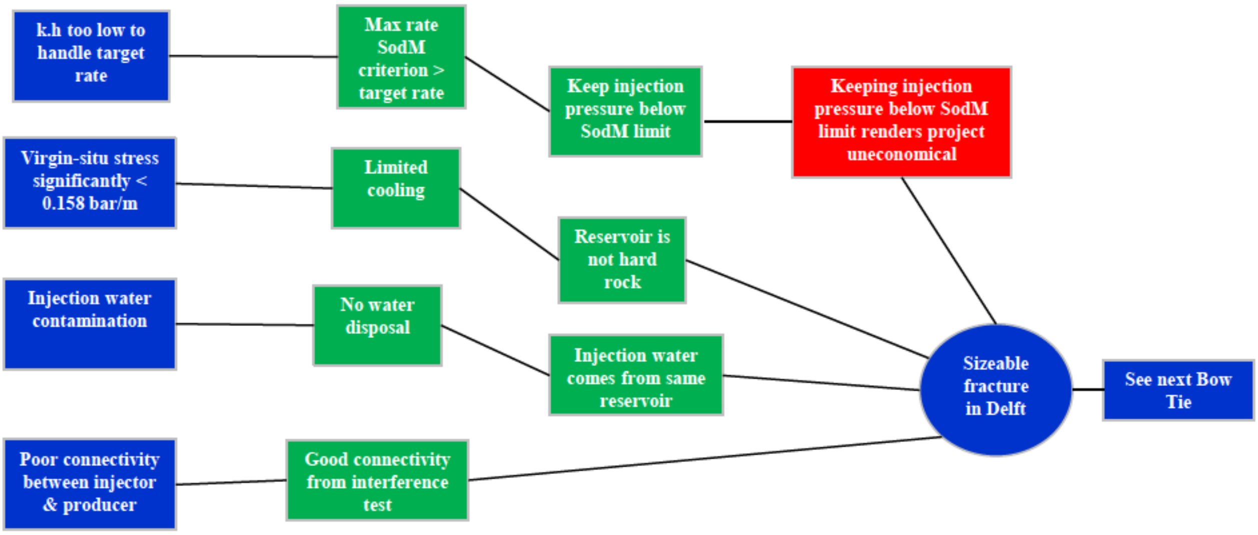

Figure 3-1: Bowtie diagram for the formation of a sizeable fracture in the Delft formation. Please also see Figure 3-2.

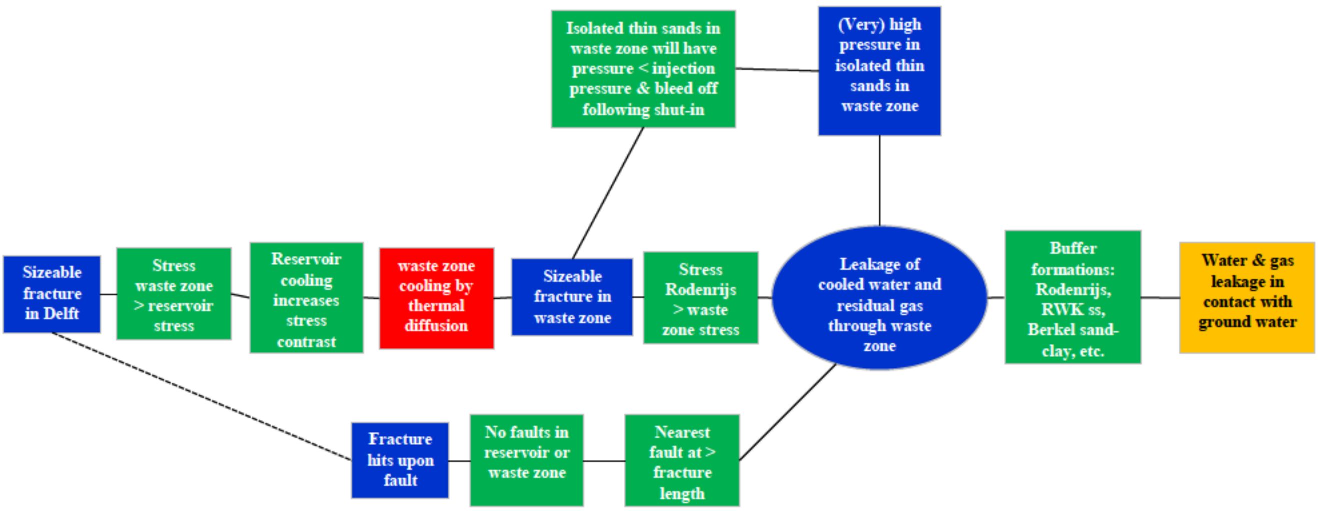

Figure 3-2: Bowtie diagram for water & gas leakage towards ground water levels once a sizeable fracture has formed in the Delft formation. Please also see Figure 3-1.

In general, the following mechanisms could affect integrity of the seal:

1. Large induced fractures carry a greater risk of growing significantly upwards into the seal. Large induced fractures are primarily a consequence of low k.h of the formation in relation to target injection rate (Figure 3-1). A first indication of this risk is provided by a figure of the type of Figure 2-1: if the maximum allowable injection rate for matrix injection (i.e. for injection pressure below the SodM limit) is significantly below the target injection rate, this may be an indication of large induced fractures when injecting at target rate. One option in a situation lke this one is to reduce injection pressure to a value below the SodM limit, but, as discussed in the introduction, this may render a project uneconomical.

2. Another mechanism that can contribute to large(r) fractures is a low fracturing pressure (Figure 3-1). This can be the consequence of a low virgin minimum in-situ total stress (mostly significantly below the value of 0.158 bar/m for an extensional regime), often in combination with significant cooling (with respect to reservoir temperature) and hard rock (meaning a high value of the thermo-elastic constant A_T). The fracturing pressure for cold water injection can be established by a step rate test. Also, analysis of operational injection data can provide an idea of whether one is injecting under induced fracturing conditions, and if yes, the fracturing pressure. This will be further discussed in the chapter about monitoring below.

3. Poor injection water quality is well-known to be a cause of large induced fractures (Figure 3-1). This is particularly pronounced for injection disposal of produced water. However, in the Dutch geothermal operations, water is injected back into the same reservoir without exposure to air, and therefore formation plugging by 'poor' quality water (including chemical incompatibility effects) is mostly absent. This has been verified by long-term injection monitoring in a number of Dutch geothermal operations.

4. Finally, large induced fractures can be the result of local reservoir pressurisation around the injector (Figure 3-1). This will typically happen when there is poor reservoir connectivity (e.g. sealing fault) between injector and producer of a doublet. Such a poor reservoir connectivity should have been established upfront by interference testing.

5. Large fractures as described above are a 'requirement' in order to have significant growth into the seal. However, even in the case of large fractures, growth into the seal may be very limited provided there is a good stress contrast between those layers (Figure 3-2). For example, when the cap rock consists of (e.g. Zechstein) salt, the stress contrast is mostly sufficiently large to prevent any substantial upward fracture growth. Very often the cap rock consists of shale. Although shales generally have a higher virgin horizontal stress than sandstones (because of higher Poisson's ratio), the resulting stress contrasts between sand and shale is often not enough to contain the fracture to the sandstone. Moreover, sand-shale stress contrasts are generally very uncertain and cannot be reliably obtained except by proper in-situ measurements (e.g. microfrac test). Therefore, in simulations we generally take the conservative value of zero sand-shale stress contrast.

6. Injection of cold water into a sandstone will lead to rapid cooling of this sandstone, whereas the overlying shale remains at virgin temperature. Therefore, even in the absence of any virgin sand-shale stress contrast, the cooling-induced stress contrast can help partial fracture containment to the sandstone reservoir (Figure 3-2). However, over time, the bottom part of the overlying shale will start

to cool as well owing to thermal diffusion, and this may lead to additional fracture extension into the bottom part of the shale (Figure 3-2). Typically, for 30-year injection about 30 m at the bottom of the caprock shale has been cooled and may also be fractured. This provides an upper limit to the upward fracture growth for large induced fractures, provided the cooling provides for enough stress contrast between sand and shale.

7. Apart from in-situ stress contrast, there may be other differences in layer properties that could (help) contain the induced fracture to the reservoir. Over the decades, there has been a lot of debate amongst experts on this point. Although the debate is still ongoing, it is generally agreed that only in-situ stress contrasts can (help) contain induced fractures with sufficient certainty. Although other physical properties (e.g. Young's modulus contrast, permeability contrast, certain properties of interfaces between layers, etc.) have been demonstrated to be effective in certain situations, the scatter in the data is too large to come up with any definitive conclusions.

8. Finally, a word about injection pressure. Generally, it can be stated that the higher the injection pressure, the higher the risk of induced fracturing. However, apart from the (conservative) SodM limit, it is not possible to define one specific injection pressure limit below which there will be no (excessive) fracturing. This is because fracturing pressure for (cold) water injection is not one steady number that will never ever change. By contrast, apart from minimum in-situ stress, temperature difference and thermo-elastic constant, it depends on the current operation (injection versus shut-in), operational history, current size of the induced fracture, and reservoir geometry. For example, under steady-state injection there is a poro-elastic contribution to the fracturing pressure that pushes it upwards, and this can be significant especially for small fractures. On the other hand, after a shut-in, the 'pressure mountain' around an injector has dissipated into the reservoir and fracturing pressure is lower. Therefore, if one wants to use an upper limit to the injection pressure for 'safe' injection, a conservative number should be used which is provided by the SodM guideline. On top of that, it is always recommended to regularly monitor and interpret injection data in order to verify whether one is injecting under matrix conditions or under fracturing conditions (see next paragraph).

3.2 Management of risks

The risk of sizeable fracture growth with possible loss of containment can be managed by a number of monitoring methods. These monitoring results can form the basis of further action (e.g. bean back) when required. In the text below, a number of monitoring methods are explained that can be performed during operation of the geothermal project. It is assumed that proper upfront data collection about the reservoir (in particular, k.h and connectivity through well test / interference test) has been carried out.

3.2.1 Hall plot

The Hall plot is a simple method to help spot changes in injectivity over time, and in particular whether induced fracturing is taking place or not. The slope of the Hall plot is an indication of the inverse injectivity. That is, a low Hall plot slope means high injectivity and vice versa. In order to observe the signature of fractured injection, one needs to plot the Hall plot and he injection rate on the same graph, see Figure 3-3 for an example. Injection under fracturing conditions can be observed from the correlation that lower injection rates lead to higher Hall plot slopes and vice versa. This can be understood by realizing that the Hall slope is roughly defined as (injection pressure) divided by (injection rate). When the injection rate is reduced, the fracture shrinks but the injection pressure remains the same (being the fracture propagation pressure). As a result, the Hall slope will increase. Similarly, increasing injection rate will result in a lowering of the Hall plot slope. In order to help spot changes in the Hall plot slope, a derivative is also included.

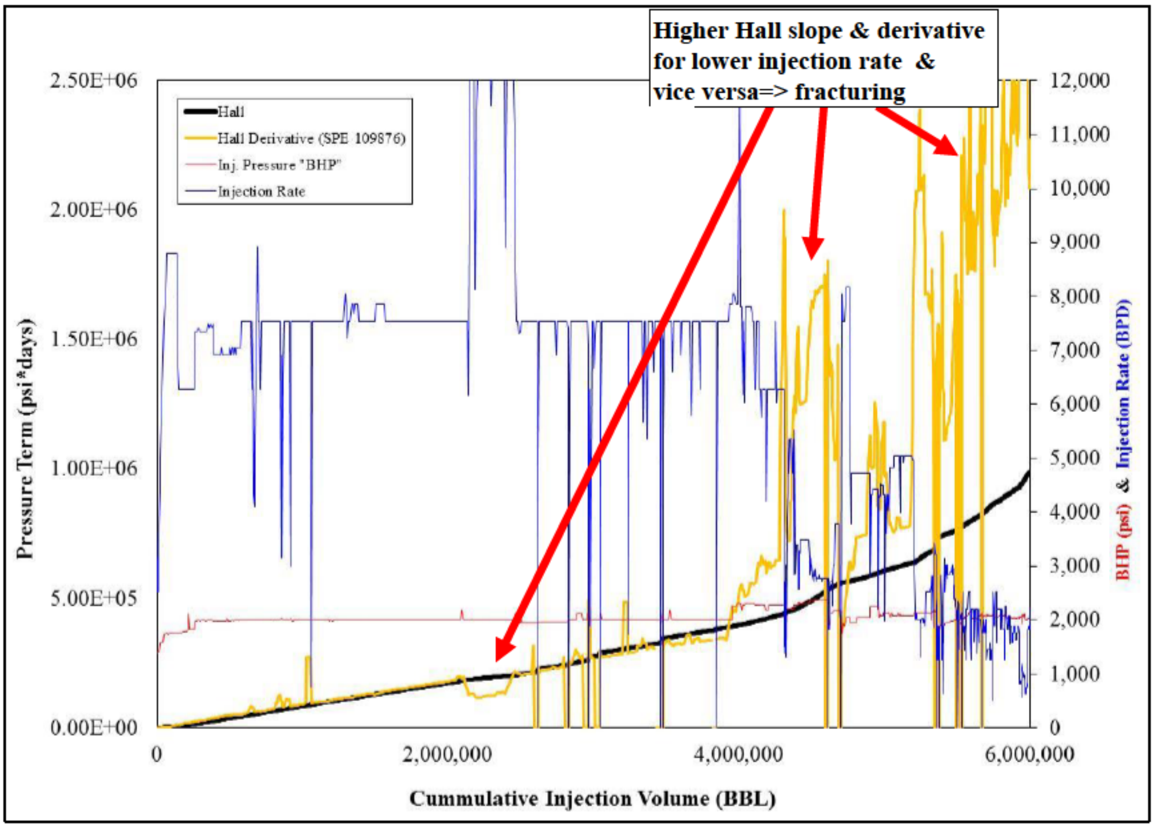

Figure 3-3: Hall plot of injection data in Oman.

For geothermal operations, the Hall plot slope can also be correlated to injection temperature to spot possible fracturing: a lower (instead of higher) Hall plot slope for lower injection temperature points in this direction. This was indeed observed in a number of geothermal cases in West Netherlands. The Hall plot methodology is being routinely applied by at least one geothermal operator in the Netherlands.

3.2.2 Injection fall-off (IFO) test

Once a Hall plot analysis points convincingly in the direction of (sustained) induced fracturing, an injection fall-off test can be carried out to estimate the size (length, height) of the induced fracture. A field example (derivative plot) is shown in Figure 3-4.

The derivative plot of an IFO test has a number of characteristic features:

- Short time: Slope on a log-log plot is equal to one: "storage dominated". For IFO, this is mainly the storage of the closing fracture. From this part, the fracture length and height are derived using the technique of *SPERE Journal, October 2005, 377-387.*

- After the storage period, the slope of the pressure derivative curve often increases to a peak value. This is the period of a shrinking (receding) fracture which precedes complete fracture closure (see *SPEPE Journal, February 2017, 1-17*). The top of the "hump" is generally associated with complete fracture closure

- After the hump has dropped, the derivative is characterised by a horizontal line. This is called "radial flow" in the reservoir and from this part the quantity k*h can be derived.

- At the end of the radial flow period, it can be seen that for this field example, the pressure derivative slowly increases to a higher value. This is because the injection water displaces crude which has a lower mobility and therefore corresponds to a higher level of the horizontal line of the pressure derivative (this particular example).

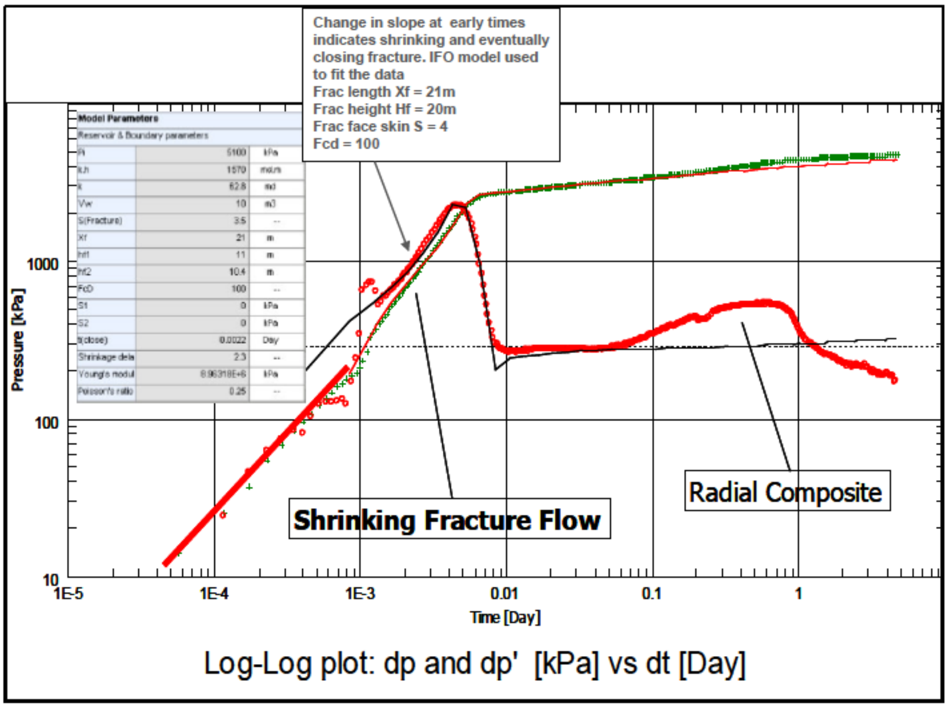

Figure 3-4: Example of derivative plot from an injection fall-off test including interpretation (Oman).

The IFO method allows one to estimate the size of the induced fracture and from that, to assess whether (significant) out-of-zone growth into the caprock could have taken place or not. Figure 3-5 shows a set of IFO tests performed over a period of a few months during a waterflood operation. Clearly, the impact of fracture growth can be observed.

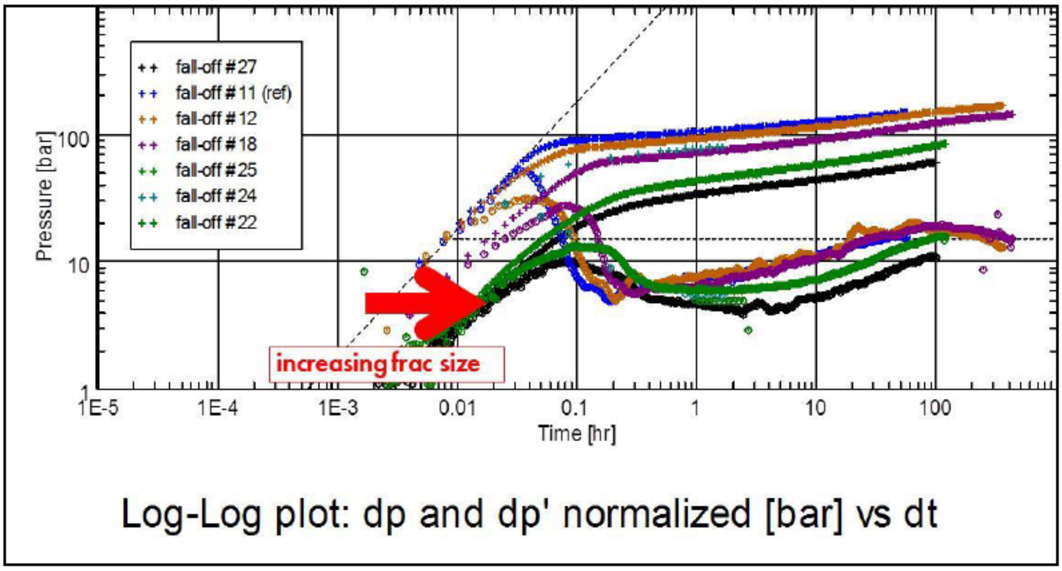

Figure 3-5: Example of IFO derivative plots performed over a couple of months (Siberia).

Based on (an) IFO measurement(s) (and possible trends therein), it can be decided to lower injection rate if significant fracture growth is observed.

3.2.3 Temperature log (warm-back survey)

If monitoring results appear to indicate that indeed sizeable fractures have been created, it may be required to 'explicitly' measure upward fracture growth. This can be done by means of a temperature log. The principle is explained in Figure 3-6.

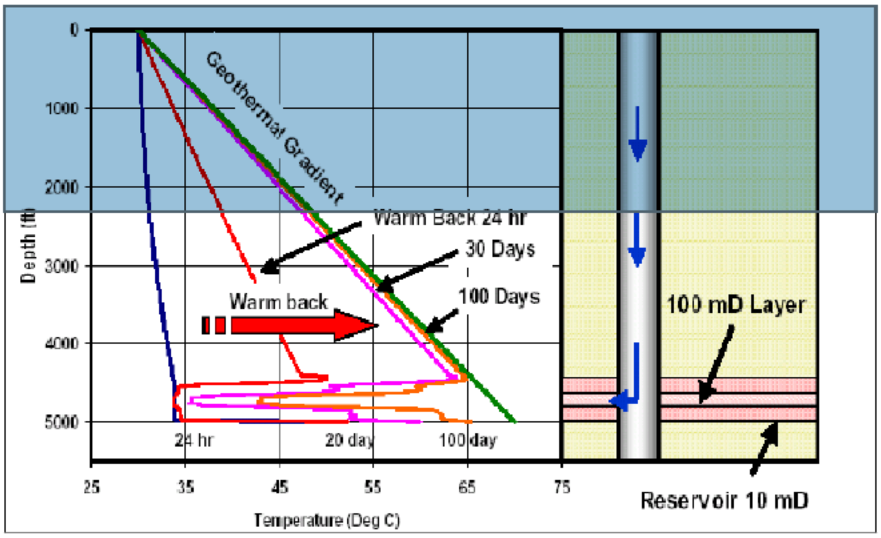

Figure 3-6: Principle of a warm-back survey.

The warmback survey consists of running a temperature log (which measures the temperature profile along the borehole) at different times after injector shut-in. What will happen is that zones that have not been flooded with (cold) injection water will warm back quickly, leaving a distinct "temperature valley" where water has flooded the reservoir. The blue, pink and red curves in the right-hand log plot show the temperature profile measured at subsequent periods after shut-in, clearly illustrating the principle.

It is important to realize that a temperature log gives a far superior measurement of which zones have been flooded than a PLT. The PLT only shows where the water leaves the well, which is different from where it floods the formation. For example, the water injection can induce a fracture which propagates into an overlying zone away from the wellbore. In such a situation, the PLT will suggest that you are flooding the right zone, whilst the temperature log / warm-back survey will show you that you flooding the wrong zone. This is actually what was observed at some stage in the BP waterfloods in the Prudhoe Bay field in Alaska.

The combination of warmback surveys and IFO is considered to be a very powerful way of monitoring induced fracture growth during waterfloods. An illustration is given in Figure 3-7, showing warm-back surveys over time for the same operation as the IFO results in Figure 3-5. Clearly, the IFO's and warm-back surveys indicate the presence of an induced fracture growing (modestly) upward from the reservoir into the overlying cap rock.

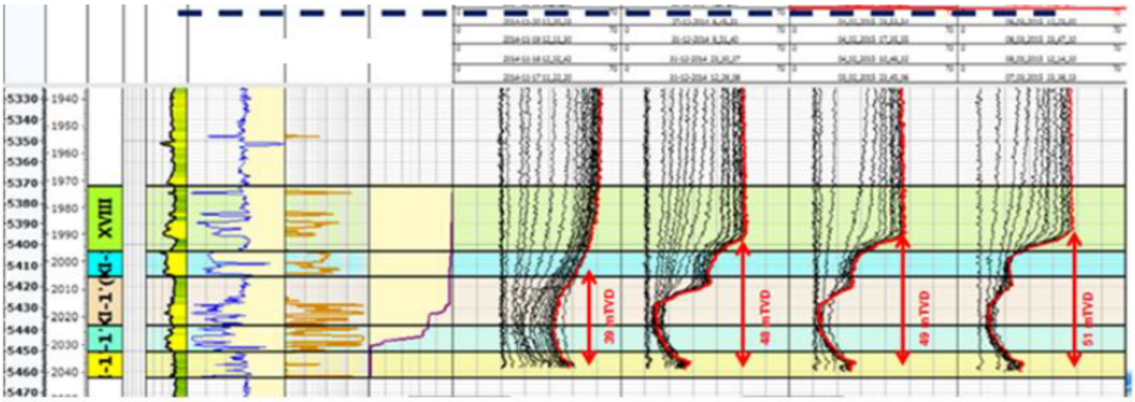

Figure 3-7: Example of warm-back surveys performed over a couple of months (Siberia, same case as Figure 3-5).

3.2.4 Summary

In summary, it is recommended to carry out Hall plot analyses on a routine basis, based on day-to-day injection data. IFO testing may be required if Hall plot analysis indicates the presence of induced fractures, though in general it is recommended to do this anyway in the early phase of the operation. Warm-back surveys will generally not be required, provided the combination Hall plot / IFO shows that induced fractures remain small.

4 Input data for fracture simulations

4.1 Description of base case

The simplified stratigraphy, as used in the fracture simulations, is depicted in Figure 4-1 below. Other main features of the base case are:

- Geological 'layer-cake' model
- Minimum horizontal in-situ stress based on general correlation for the West-Netherlands Basin (Verweij et al., see also below).
- No in-situ stress differences between sand layers and shale layers. This can be considered as a 'conservative' approach in the sense that normally, sandstone formations have a lower horizontal in-situ stress than shale layers. As a result of the higher in-situ stress in the shale, (thermal) fractures that are induced in sandstones will often be (partially) contained by the bounding shales
- Hydraulic formation pressure gradient
- Elastic parameters of the rock (Young's modulus, Poisson's ratio) based on general geomechanical correlations and NLW-GT-03-S1 / NLW-GT-01 shear sonic data
- A permeability of 700 mD is used as input for the Delft reservoir in NLW-GT-01 and of 800 mD in NLW-GT-04. These values are based on well test results. All other permeabilities are from ThermoGIS database.
- All geological layers are continuous with a constant pressure boundary at the drainage radius (= ½ × distance between wells of the doublet)
- Water is injected at 2315 m TVD (2 m below top reservoir) for NLW-GT-01 and at 2234 m TVD for NLW-GT-04.
- Injection rate is 430 m3/hr during 30 years for NLW-GT-01, and 300 m3/hr during 30 years for NLW-GT-04.

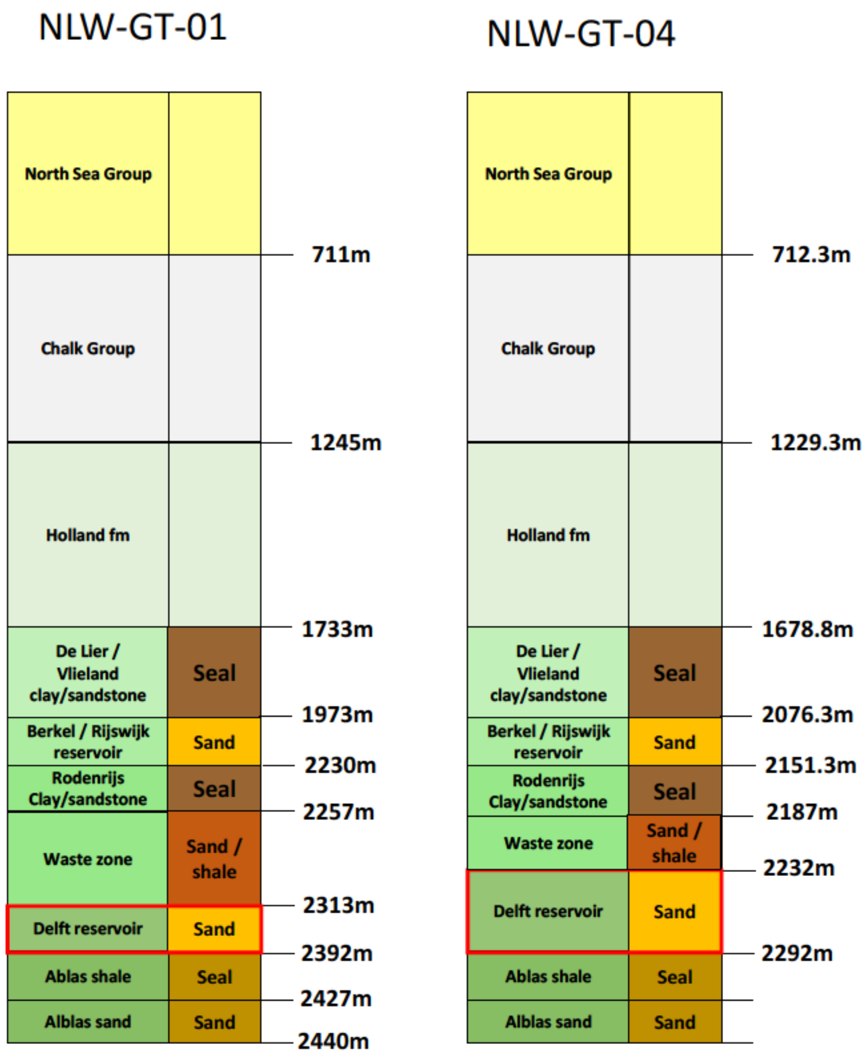

Figure 4-1: Stratigraphy in NLW-GT-01 and NLW-GT-04.

4.2 In-situ stress estimate

In-situ stress trends are mostly based on measured leak-off pressures as reported by Verweij et al. (2012). These authors distinguished a number of different geological areas within the Netherlands. For each of these areas, an in-situ stress trend map was generated. The geological area that is relevant for the current discussion is the so-called West Netherlands Basin for which the data are given in figure 4-2. This figure displays measured Formation Integrity Tests (FIT) / leak-off pressure tests (LOT) as a function of depth in the West Netherlands platform area.

Until a depth of around 1500 m, the trend closely follows the well-known minimum in-situ stress gradient of 0.158 bar/m (0.7 psi/ft) for an extensional stress regime, whilst at greater depths it starts to bend somewhat towards higher stresses.

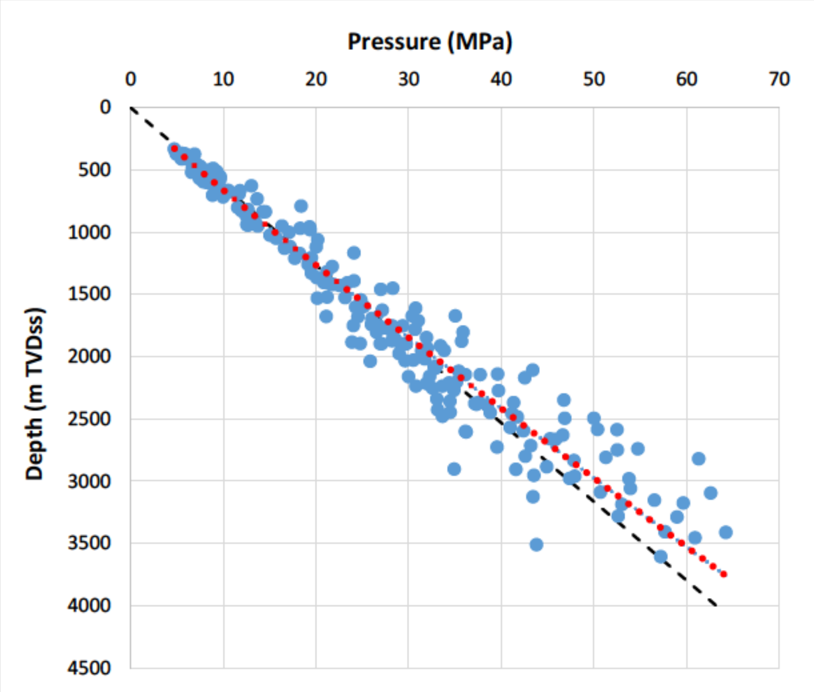

Figure 4-2: Minimum in-situ stress versus depth trend in the West Netherlands Basin area based on Formation Integrity Tests (FIT) / Leak-Off Tests (Verweij et al, 2012). Red-dashed line: trend line based on leak-off tests. Black-dashed line: trend line of 0.158 bar/m.

From the dataset shown in Figure , a subset was chosen from wells in the neighborhood of Trias Westland. The wells chosen plus the resulting stress trend are displayed in Figure . As can be seen, the baseline trend falls more or less on top of the well-known trend of 0.158 bar/m for an extensional stress regime, with a standard deviation of 0.02 bar/m.

The caprocks immediately above the target injection zone (Delft) consist of shale. Although shales generally have a higher virgin horizontal stress than sandstones (because of higher Poisson's ratio), the resulting stress contrasts between sand and shale is often not enough to contain the fracture to the sandstone. Moreover, sand-shale stress contrasts are generally very uncertain and cannot be reliably obtained except by proper in-situ measurements (e.g. microfrac test). Therefore, in the simulations presented below, we take the conservative value of zero sand-shale stress contrast as a base case.

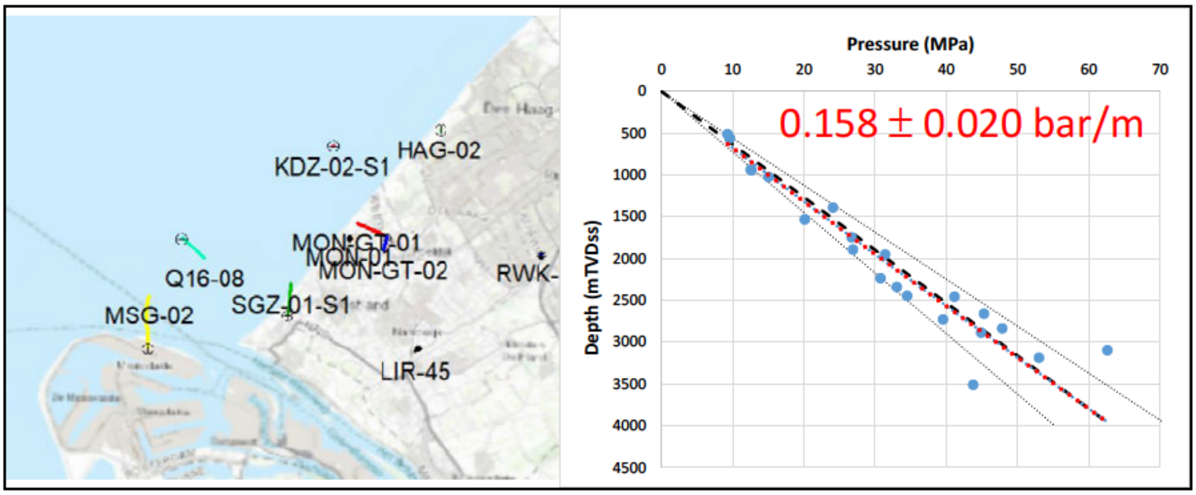

Figure 4-3: Minimum in-situ stress versus depth trend in the West Netherlands Basin area based on Formation Integrity Tests (FIT) / Leak-Off Tests from wells in the neighborhood of Trias Westland.

4.3 Physical rock parameters

4.3.1 Permeability

As mentioned in chapter 3 above, for fracture containment around an injector in a geothermal setting, the most critical physical rock parameter is permeability. High(er) permeability leads to smal(ler) fractures, whereas low(er) permeability leads to large(r) fractures. Resulting fracture dimensions can differ up to several orders of magnitude when going from high tot low formation permeabilities.

4.3.2 Thermo-elastic constant

In response to temperature changes, the reservoir rock will tend to expand (heating) or shrink (cooling). Because in the subsurface there is no 'room' in the horizontal direction to expand or shrink ('plane strain'), this results in a change of total horizontal stress that is given by

$$\Delta\sigma_{\mathrm{h}} = A_{\mathrm{T}}.\Delta T \qquad (1)$$

where ΔT is the temperature change (negative for cooling) and A_T is the "thermo-elastic constant" (in bar/°C). Equation (1) is only valid if the entire reservoir has been cooled. When only part of the reservoir has been cooled, a geometry correction factor is applied. This geometry correction factor is also included in the fracture simulator.

The thermo-elastic constant is a material property of the rock. Under the assumption of perfectly elastic behaviour of the rock, both at matrix level and at grain level, this constant can be expressed as

$$A_{\mathrm{T}} = \frac{\alpha E}{1-\nu} \qquad (2)$$

where

- α is the linear thermal expansion coefficient (in $°C^{-1}$)
- E is Young's modulus (in bar)
- ν is poisson's ratio (dimensionless)

suggesting that A_T is linearly proportional to Young's modulus E if the thermal expansion coefficient α is assumed equal for all types of rocks under all circumstances (stress, temperature, ..).

Not many measurements of this constant have been carried out. Koning (1988) and Perkins and Gonzalez (1985) used values for A_T in the range 0.9-1.0 bar/°C for 'medium-strength' reservoir sandstones with Young's moduli in the range 10-15 GPa. For deep, tight rocks (> 10000 ft TVD), values of A_T in the range 1.5-2.0 bar/°C have been used in a number of oil field studies with waterflooding, both in Prudhoe Bay, Alaska (Stevens et al, 2000) and in the North Sea (Svendson et al, 1991, Santarelli et al, 2008). On the other hand, in the Eider oil field, North Sea (~ 9000 ft TVss) a value of A_T = 0.6 bar/°C was derived based on step-rate tests, whilst in a carbonate / mudstone reservoir in the Middle East (~6500 ft tVD), a range of 0.4-0.9 bar/°C was measured on different core plugs. From the above we derive an average value for A_T of ~1.0 ± 0.5 bar/°C, which may increase up to ~ 2,0 bar/°C for (very) tight rocks. In the current study a value of 1.0 ± 0.5 bar/°C is used.

4.3.3 Poro-elastic constant

In response to pressure changes, the reservoir rock will tend to expand (pressurisation) or shrink (depletion). Because in the subsurface there is no 'room' in the horizontal direction to expand or shrink ('plane strain'), this results in a change of total horizontal stress that is given by

$$\Delta\sigma_{\mathrm{h}} = A_{\mathrm{p}}.\Delta p \qquad (3)$$

where Δp is the pressure change (negative for depletion) and A_p is the "poro-elastic constant" (dimensionless). Equation (3) is only valid if the entire reservoir has been pressurised or depleted. When only part of the reservoir has been pressurised / depleted, a geometry correction factor is applied. This geometry correction factor is also included in the fracture simulator.

The poro-elastic constant is a material property of the rock. Under the assumption of perfectly elastic behaviour of the rock, both at matrix level and at grain level, this constant can be expressed as

$$A_{\mathrm{p}} = (1-\beta)\frac{1-2\nu}{1-\nu} \qquad (4)$$

where

- $\beta = \frac{K_m}{K_s}$
- K_{m} is the bulk modulus of the rock matrix (bar)
- K_{s} is the bulk modulus of the solid rock grains (bar)

In practice, the above equation is only of qualitative value. Laboratory tests have shown that A_p often deviates significantly from the formula (4). Typical values are in the range 0.5-0.8. In the current study a value of 0.6 is used. Contrary to the thermo-elastic constant A_T, the value used for A_p is less critical because in a typical geothermal doublet, only a very small area around the injector is pressurised and only a small area around the producer is "depleted". On the other hand, a significant area around the injector will be cooled during the field life, thus making the parameter A_T a more critical one.

4.3.4 Young's modulus and Poisson's ratio

Fracture dimensions are only indirectly dependent on Young's modulus and Poisson's ratio, i.e. only variations in these parameters between different geological layers can help (temporarily) contain fractures. First, contrast in Young's modulus / Poisson's ratio between different layers can result in stress concentrations when the fracture tip approaches a layer boundary, and this can retard vertical fracture growth. This mechanism is included on the fracture simulator. Secondly, contrast in Young's modulus / Poisson's ratio between different layers could result in different thermo-elastic stress changes for different layers, see equation (1). One problem with simulating this effect is that the thermal expansion coefficients α for the different layers are unknown, and therefore estimation of A_T for each layer is difficult. Because of this problem, in the current study the impact of layering on A_T has not been addressed.

Young's modulus and Poisson's ratio for all layers were derived from compressional and shear sonic logs measured in Trias Westland wells GT01 and GT03.

5 Description of the fracture model and uncertainties

5.1 Model description

Fracture simulations were performed using the methodology of Gheissary (1998) and van den Hoek (1999,2000). This is an extension of the Koning method (Koning, 1988) that is also used by TNO (Veldkamp et al., 2016), including more complicated geologies with multiple layers of reservoir and cap rock. This model was extensively applied in the field, and also validated against other models and against field data.

5.2 Model uncertainty

The main shortcoming of the simulator is that it uses an assumed fracture shape (planar vertical fracture consisting of two vertical half-ellipses). Thus, a horizontally symmetric fracture around the injection point is assumed. In practice, this shortcoming has turned out to be of limited consequence (i.e. limited with respect to geological and parameter uncertainties), as was shown by many validations.

5.3 Base case/simplified stratigraphy

The simplified stratigraphies as used in the fracture simulations are depicted in **Error! Reference source not found.**. An overview of the geological input parameters for the base case is shown in Table 5-1 for NLW-GT-01 and Table 5-1 for NLW-GT-04.

Table 5-1: Overview of layers used in the model plus their physical parameters for NLW-GT-01. Note that the permeability in the Delft is N/G corrected.

Layer name	Depth at top (m)	Depth at bottom (m)	Stress at top (Mpa)	Stress at bottom (Mpa)	Stress gradient (kPa/m)	Form. pressure at top (Mpa)	Form pressure at bottom (Mpa)	Form pressure gradient gradient (kPa/m)	Permeability (mD)	Porosity (fraction)	Young's modulus (Mpa)	Poisson's ratio
North Sea	0	711	0	11.2338	15.8	0	7.6788	10.8	436	0.3	5912.8	0.18552
Chalk	711	1245	11.2338	19.671	15.8	7.6788	13.446	10.8	1	0.05	3220.12	0.03371
Holland	1245	1733	19.671	27.3814	15.8	13.446	18.7164	10.8	7	0.15	3792.42	0.13296
De Lier sandstone	1733	1871	27.3814	29.5618	15.8	18.7164	20.2068	10.8	1	0.15	14347.5	0.285105
Vlieland claystone	1871	1973	29.5618	31.1734	15.8	20.2068	21.3084	10.8	0.1	0.01	15110.5	0.277493
Berkel sandstone	1973	2051	31.1734	32.4058	15.8	21.3084	22.1508	10.8	2	0.15	17191	0.27101
Berkel sand-claystone	2051	2213	32.4058	34.9654	15.8	22.1508	23.9004	10.8	0.1	0.2	15914.2	0.278185
Rijswijk sandstone	2213	2230	34.9654	35.234	15.8	23.9004	24.084	10.8	10	0.15	18466	0.28408
Rodenrijs claystone	2230	2257	35.234	35.6606	15.8	24.084	24.3756	10.8	0.1	0.2	5029.87	0.315563
Waste zone	2257	2313	35.6606	36.5454	15.8	24.3756	24.9804	10.8	10	0.15	16710.8	0.288879
Delft sandstone	2313	2392	36.5454	37.7936	15.8	24.9804	25.8336	10.8	700	0.19	19260	0.225133
Alblas shale	2392	2427	37.7936	38.3466	15.8	25.8336	26.2116	10.8	0	0.01	20644	0.245774
Alblas sand	2427	2440	38.3466	38.552	15.8	26.2116	26.352	10.8	200	0.17	20644	0.245774
Alblas shale 2	2440	2517	38.552	39.7686	15.8	26.352	27.1836	10.8	0	0.01	20644	0.245774
Alblas sand / shale	2517	2650	39.7686	41.87	15.8	27.1836	28.62	10.8	50	0.1	20644	0.245774
Lower Alblas sands	2650	2751	41.87	43.4658	15.8	28.62	29.7108	10.8	50	0.1	20644	0.245774
Altena	2751	3713	43.4658	58.6654	15.8	29.7108	40.1004	10.8	0	0.01	20644	0.245774

Table 5-2: Overview of layers used in the model plus their physical parameters for NLW-GT-04. Note that the permeability in the Delft is N/G corrected.

Layer name	Depth at top (m)	Depth at bottom (m)	Stress at top (Mpa)	Stress at bottom (Mpa)	Stress gradient (kPa/m)	Form. pressure at top (Mpa)	Form pressure at bottom (Mpa)	Form pressure gradient gradient (kPa/m)	Permeability (mD)	Porosity (fraction)	Young's modulus (Mpa)	Poisson's ratio
North Sea	0	712.3	0	11.25434	15.8	0	7.69284	10.8	436	0.3	5912.8	0.18552
Chalk	712.3	1229.3	11.25434	19.42294	15.8	7.69284	13.27644	10.8	1	0.05	3220.12	0.03371
Holland	1229.3	1678.8	19.42294	26.52504	15.8	13.27644	18.13104	10.8	7	0.15	3792.42	0.13296
De Lier sandstone	1678.8	1838.3	26.52504	29.04514	15.8	18.13104	19.85364	10.8	1	0.15	14347.5	0.285105
Vlieland claystone	1838.3	2076.3	29.04514	32.80554	15.8	19.85364	22.42404	10.8	0.1	0.01	15110.5	0.277493
Berkel sandstone	2076.3	2087.3	32.80554	32.97934	15.8	22.42404	22.54284	10.8	2	0.15	17191	0.27101
Berkel sand-claystone	2087.3	2131.3	32.97934	33.67454	15.8	22.54284	23.01804	10.8	0.1	0.2	15914.2	0.278185
Rijswijk sandstone	2131.3	2151.3	33.67454	33.99054	15.8	23.01804	23.23404	10.8	10	0.15	18466	0.28408
Rodenrijs claystone	2151.3	2187	33.99054	34.5546	15.8	23.23404	23.6196	10.8	0.1	0.2	5029.87	0.315563
Waste zone	2187	2232	34.5546	35.2656	15.8	23.6196	24.1056	10.8	10	0.15	16710.8	0.288879
Delft sandstone	2232	2292	35.2656	36.2136	15.8	24.1056	24.7536	10.8	800	0.19	19260	0.225133
Underburden	2292	3000	36.2136	47.4	15.8	24.7536	32.4	10.8	0.1	0.01	20644	0.245774

5.4 Investigated scenarios

In both NLW-GT-01 and NLW-GT-04, the following sensitivities have been addressed:

No	Description	Motivation
1	Low permeability of injection zone	Lower bound of permeability uncertainty
2	Low in-situ stress gradient (0.138 bar/m)	See 3.2
3	High in-situ stress gradient (0.178 bar/m)	See 3.2
4	High injection rate	Upper bound of planned injection rate because of seasonal variations
5	Thermo-elastic constant A_T = 1.5 bar/°C	See 3.3.2

6 Modelled expected fractures and uncertainties

6.1 Injector NLW-GT-01

6.1.1 Base case

Results for the base case are shown in Figure 6-1. In this case, the induced fracture initiates from the top at 2315 m (i.e., 2 m below the Top Delft) and grows slowly up towards the boundary with the overlying waste zone at 2313 m, although it does not grow into the waste zone. The resulting fracture after 30 years of injection is about 2 m long. This is in line with the fact that for 430 m^3/hr, it is well possible to inject under matrix conditions (see Figure 2-1). In this context, it should be remarked that the fracture propagation model does not take into account the impact of fluid loss into the formation via the wellbore. The simulated fracture of 2 m radius has approximately the same surface area as the contact area of the wellbore with the formation, confirming that in the base case matrix injection is possible.

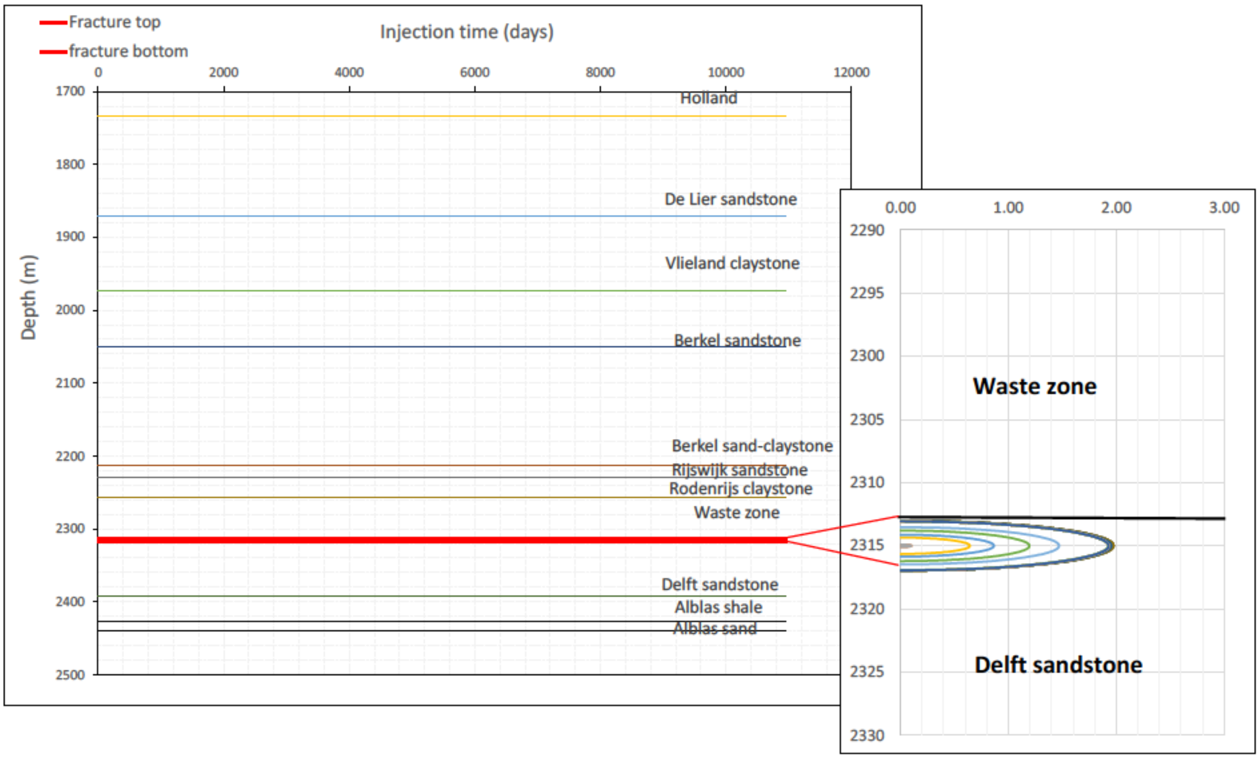

Figure 6-1: Fracture top and bottom as a function of time and fracture contours for base case.

6.1.2 Sensitivities

An overview of the addressed sensitivities plus a summary of the results for each sensitivity is given in the table below (

Table 6-1). Figure 6-2 to Figure 6-6 show more detailed results.

Table 6-1: Injection into Delft: Sensitivities+Results for well NLW-GT-01.

Sensitivity	Scenario description	Result after 30 years
0	Base case	Fracture with a length of 2 m no penetration into "waste zone".
1	Low permeability (350 mD)	Fracture with a length of 7 m with 4 m penetration into the "waste zone".
2	Low in-situ stress gradient (0.138 bar/m)	Fracture with a length of 9 m with 5 m penetration into the "waste zone".
3	High in-situ stress gradient (0.178 bar/m)	Fracture with a length of 1 m no penetration into the "waste zone".
4	High injection rate of 550 m^3/h	Fracture with a length of 3 m with 1 m penetration into the "waste zone".
5	A thermo-elastic constant A_T = 1.5 bar/°C	Fracture with a length of 4 m with 2 m penetration into the "waste zone"..

From the table and the results as presented in Figure 6-2 to Figure 6-6, the conclusion can be drawn that induced fractures for all cases remain small (< 10 m), with only a few meters upwards penetration into the waste zone.

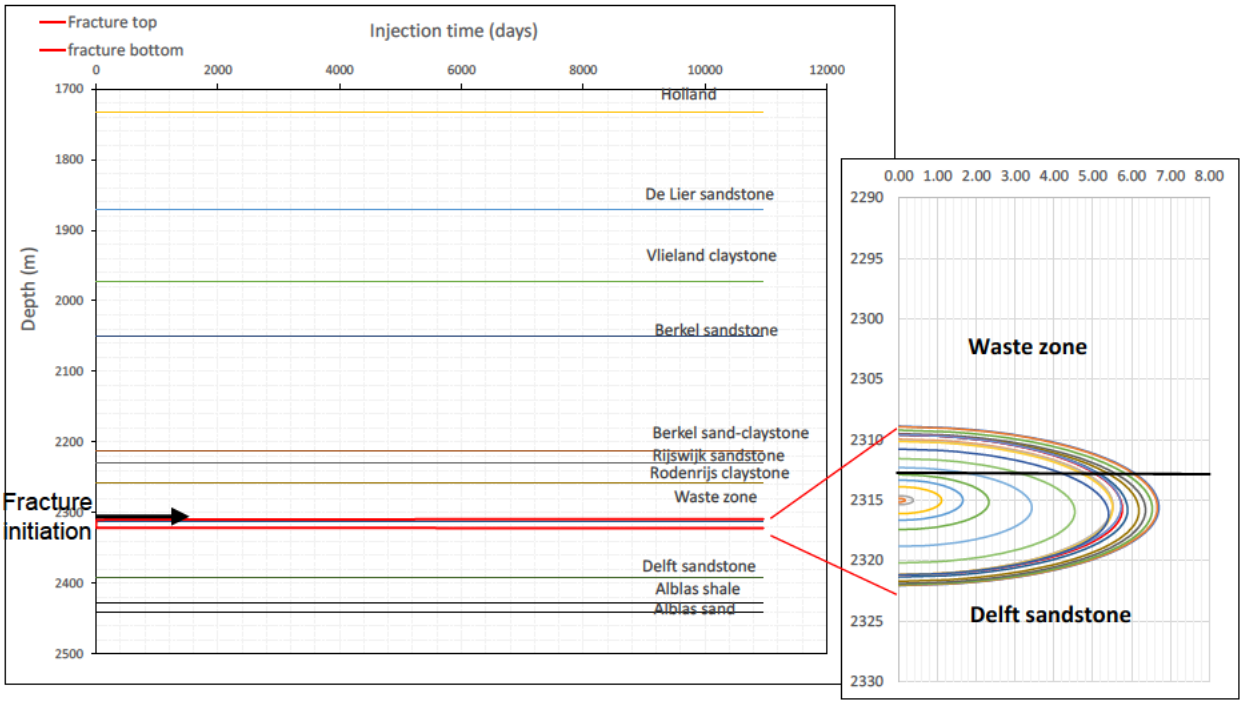

Figure 6-2: Fracture top and bottom as a function of time and fracture contours for sensitivity 1.

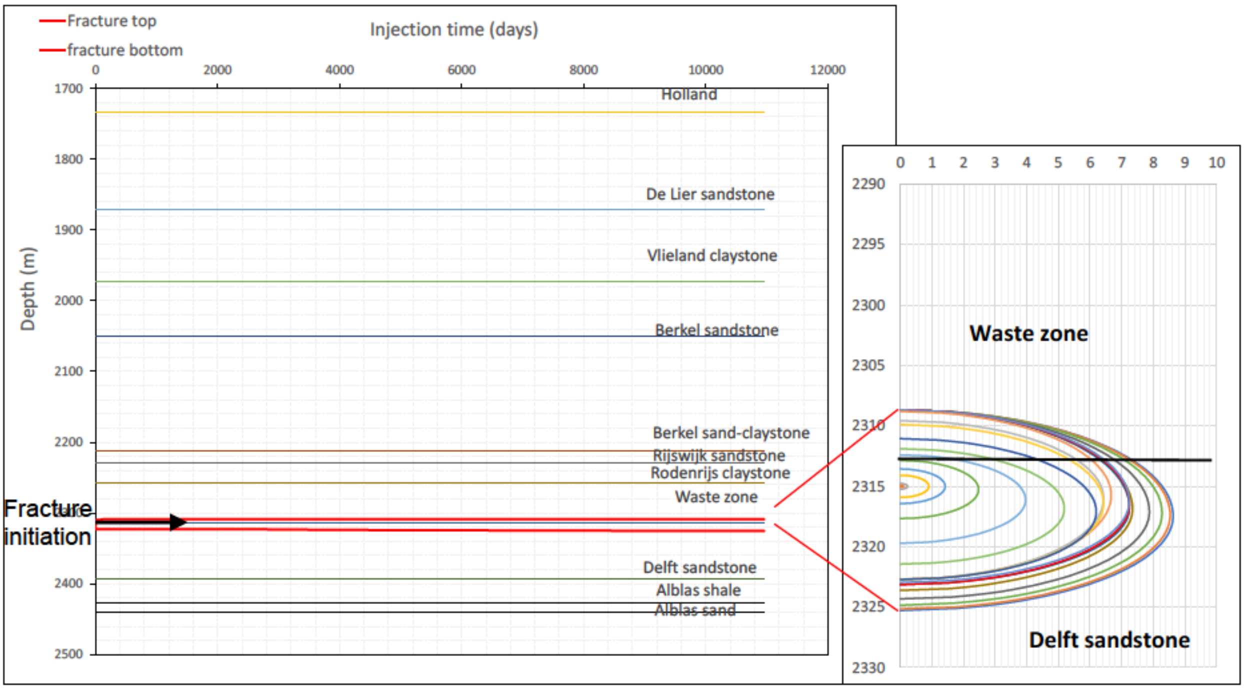

Figure 6-3: Fracture top and bottom as a function of time for base case; fracture contours for sensitivity 2.

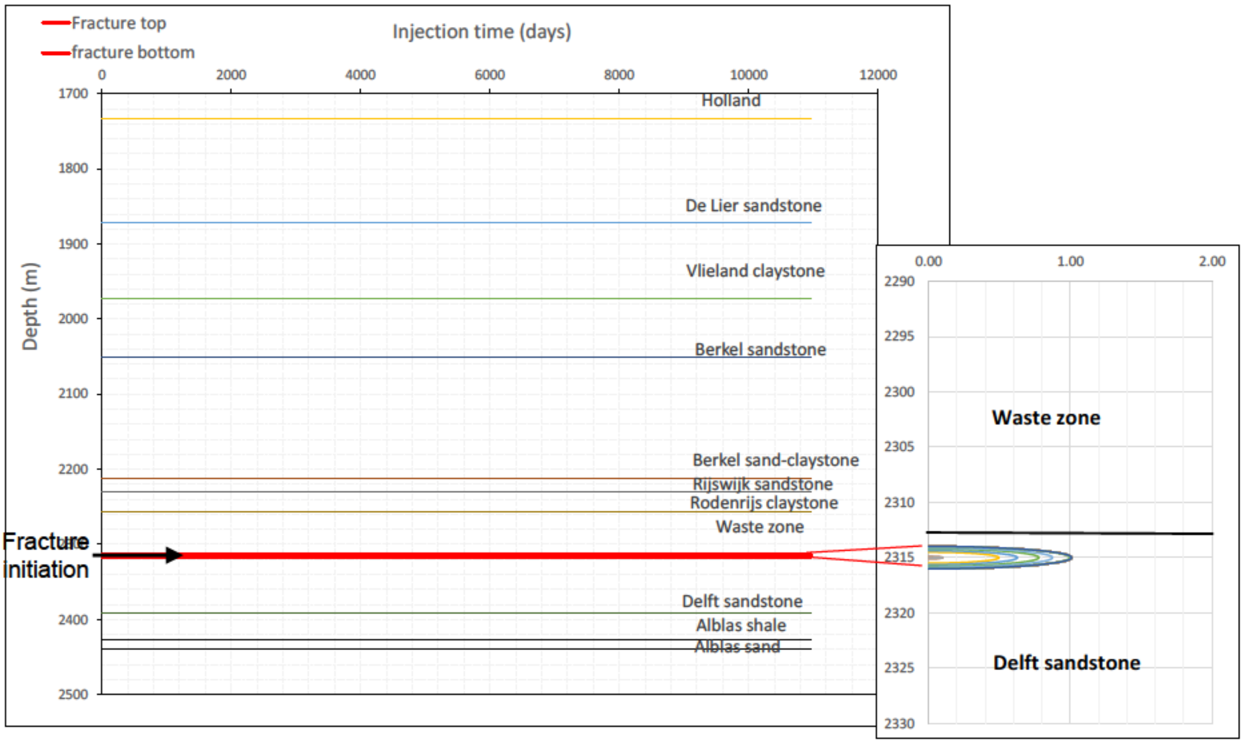

Figure 6-4: Fracture top and bottom as a function of time for base case; fracture contours for sensitivity 3.

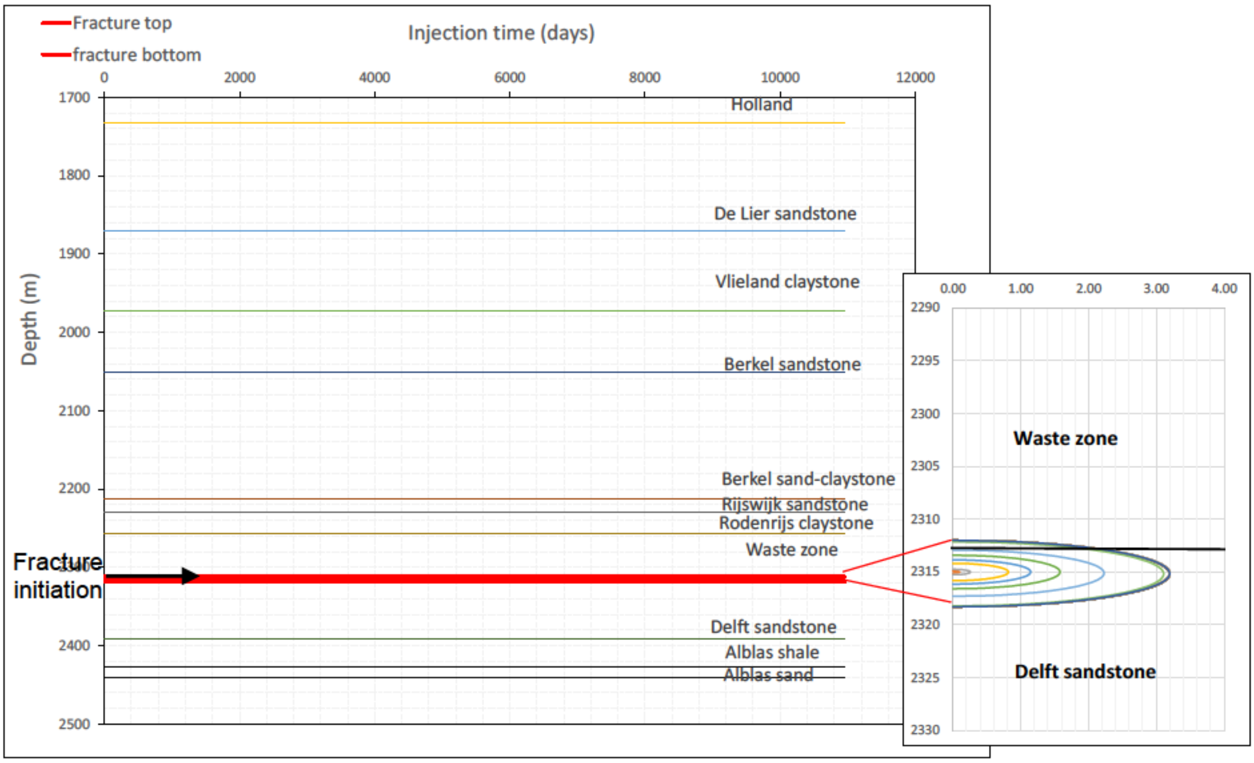

Figure 6-5: Fracture top and bottom as a function of time for base case; fracture contours for sensitivity 4.

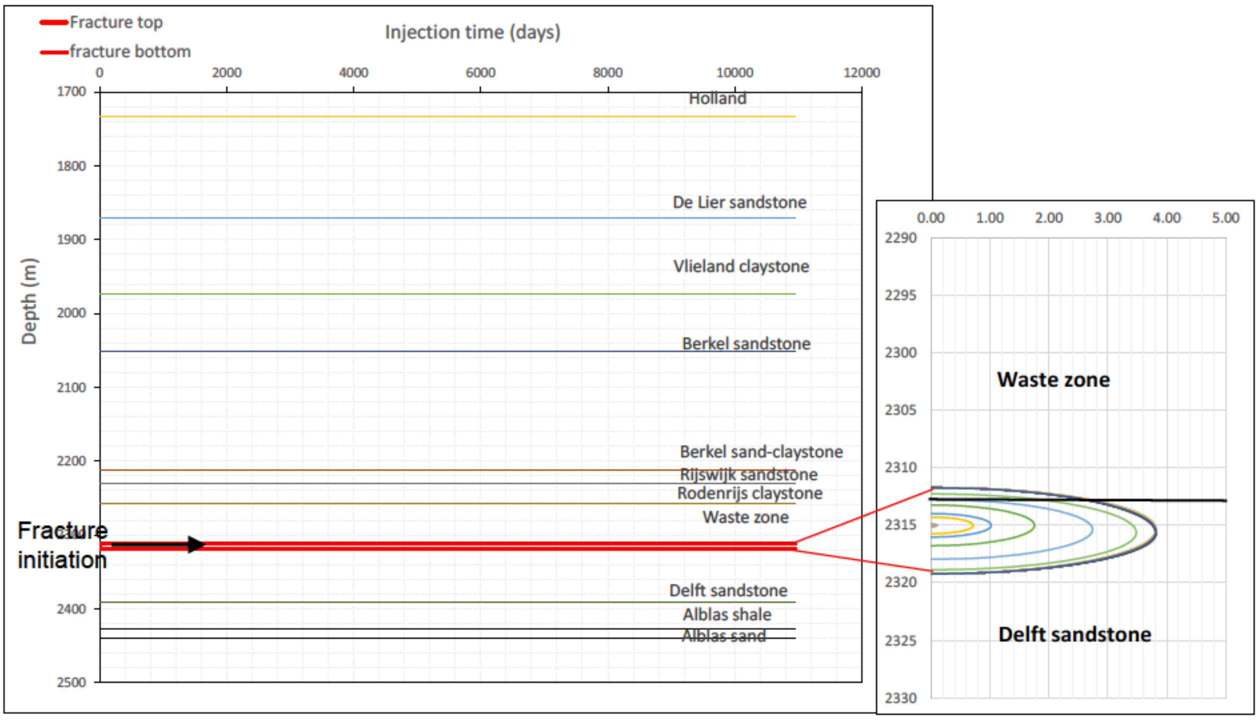

Figure 6-6: Fracture top and bottom as a function of time for base case; fracture contours for sensitivity 5.

6.2 Injector NLW-GT-04

6.2.1 Base case

Results for the base case are shown in Figure 6-7. In this case, the induced fracture initiates from the top at 2234 m (i.e., 2 m below the Top Delft) and grows slowly up towards the boundary with the overlying waste zone at 2232 m, although it does not grow into the waste zone. The resulting fracture after 30 years of injection is about 1.2 m long. This is in line with the fact that for 400 m^3/hr, it is well possible to inject under matrix conditions (see Figure 2-1). In this context, it should be remarked that the fracture propagation model does not take into account the impact of fluid loss into the formation via the wellbore. The simulated fracture of 1.4 m radius has approximately the same surface area as the contact area of the wellbore with the formation, confirming that in the base case matrix injection is possible.

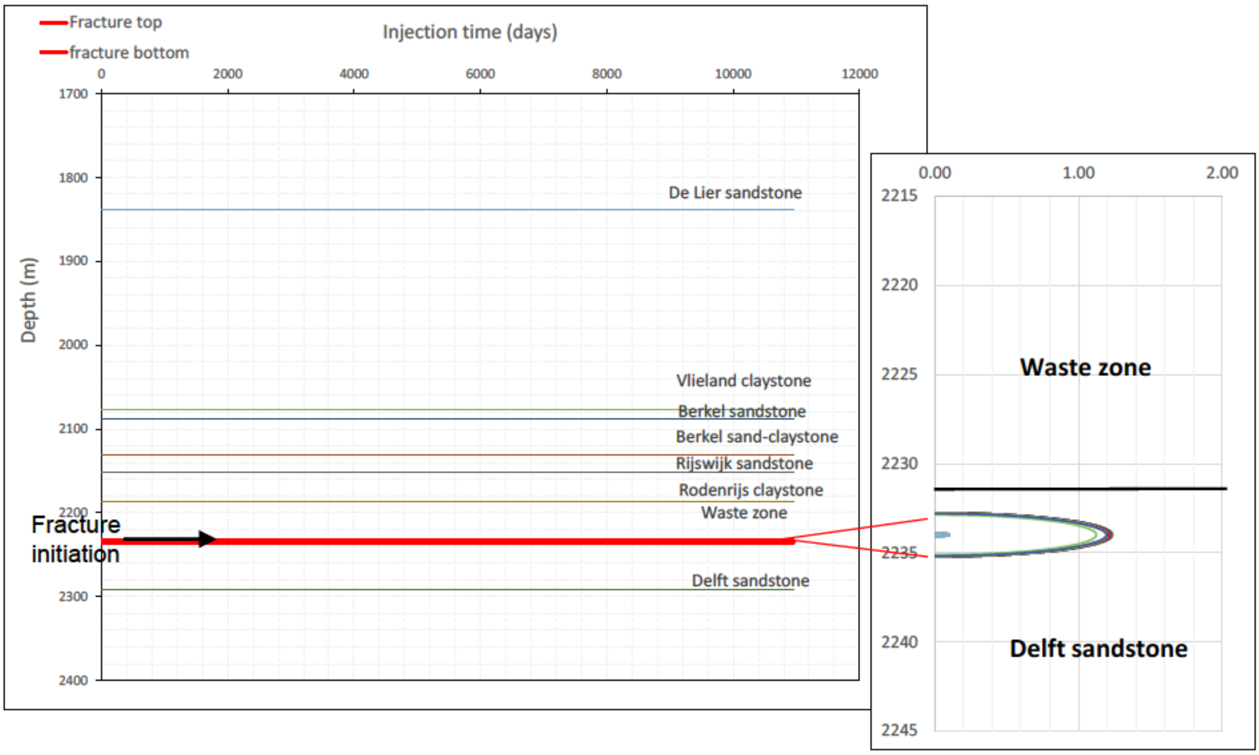

Figure 6-7: Fracture top and bottom as a function of time and fracture contours for base case.

6.2.2 Sensitivities

An overview of the addressed sensitivities plus a summary of the results for each sensitivity is given in the table below (

Table 6-1). Figure 6-8 to Figure 6-12 show more detailed results.

Table 6-2: Injection into Delft: Sensitivities+Results for well NLW-GT-04.

Sensitivity	Scenario description	Result after 30 years
0	Base case	Fracture with a length of 1.2 m no penetration into “waste zone”.
1	Low permeability (400 mD)	Fracture with a length of 4 m with 1 m penetration into the “waste zone”.
2	Low in-situ stress gradient (0.138 bar/m)	Fracture with a length of 5 m with 2 m penetration into the “waste zone”.
3	High in-situ stress gradient (0.178 bar/m)	Fracture with a length of 0.8 m no penetration into the “waste zone”.
4	High injection rate of 400 m^3/h	Fracture with a length of 1.4 m no penetration into the “waste zone”.
5	A thermo-elastic constant A_T = 1.5 bar/°C	Fracture with a length of 3 m no penetration into the “waste zone”..

From the table and the results as presented in Figure 6-1 to Figure 6-12, the following conclusions can be drawn that induced fractures for all cases remain small (< 10 m), with only a few meter upwards penetration into the waste zone. These conclusions are very similar to those of NLW-GT-01.

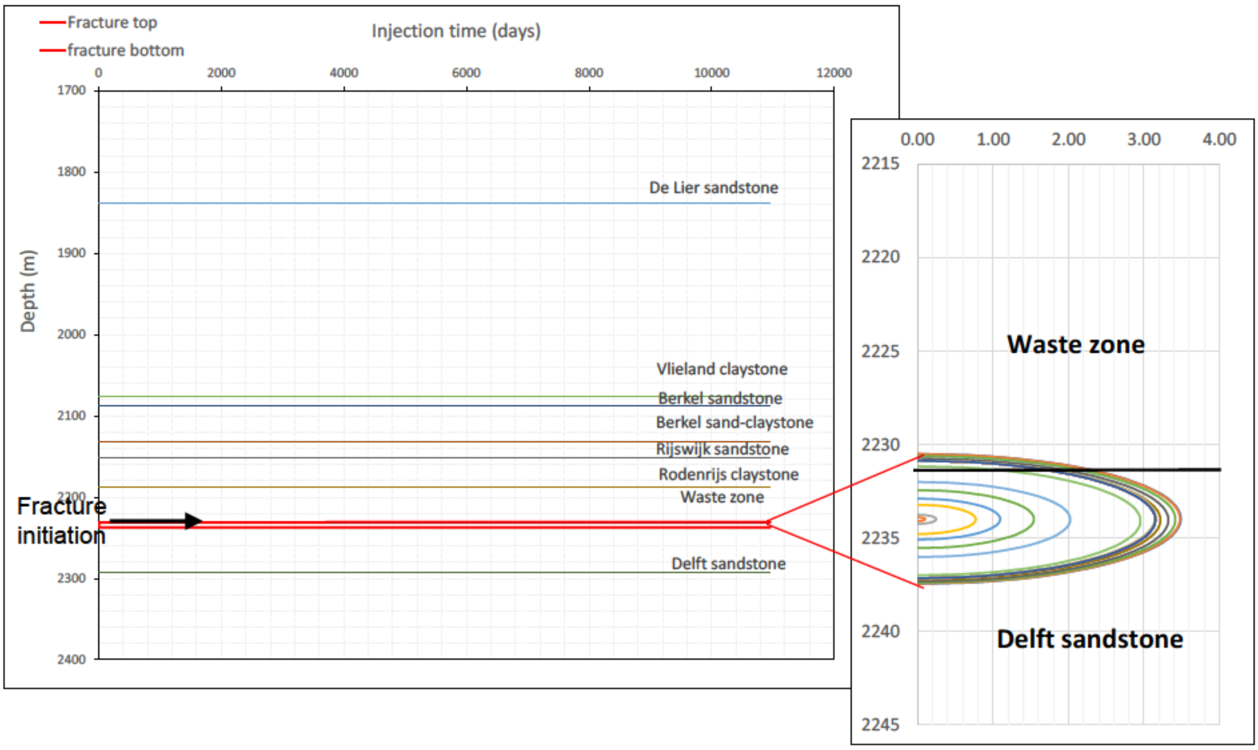

Figure 6-8: Fracture top and bottom as a function of time and fracture contours for sensitivity 1.

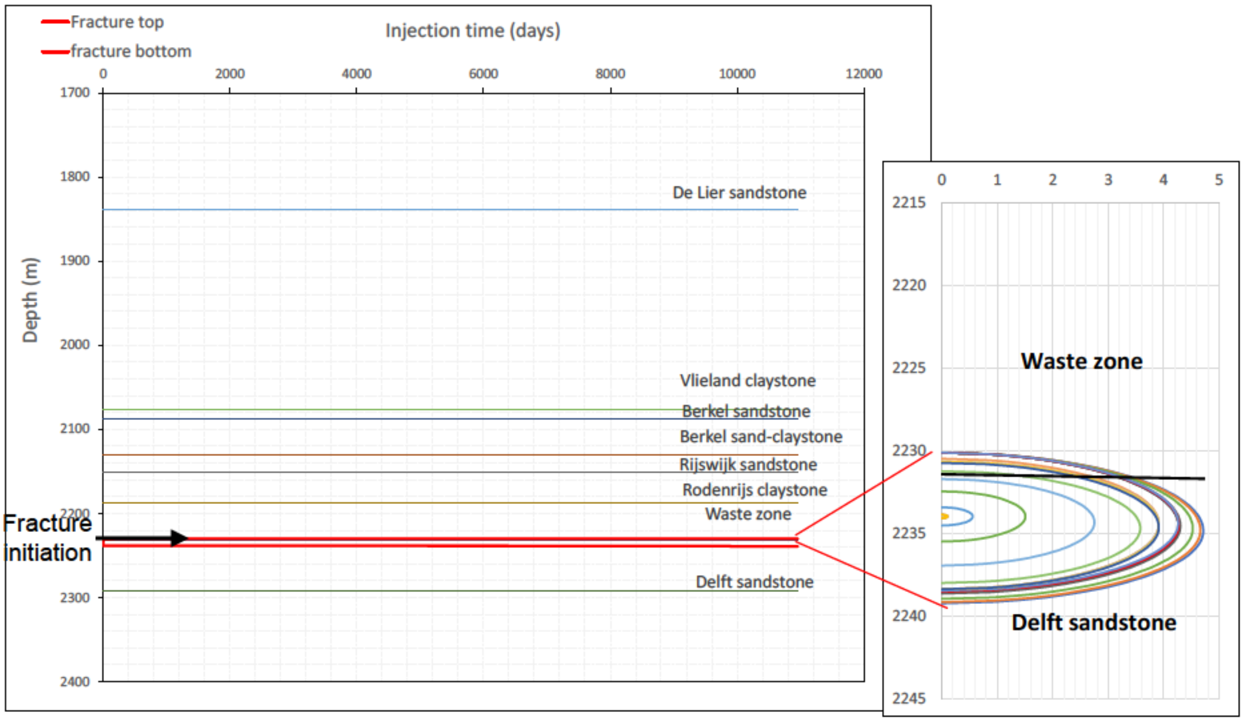

Figure 6-9: Fracture top and bottom as a function of time for base case; fracture contours for sensitivity 2.

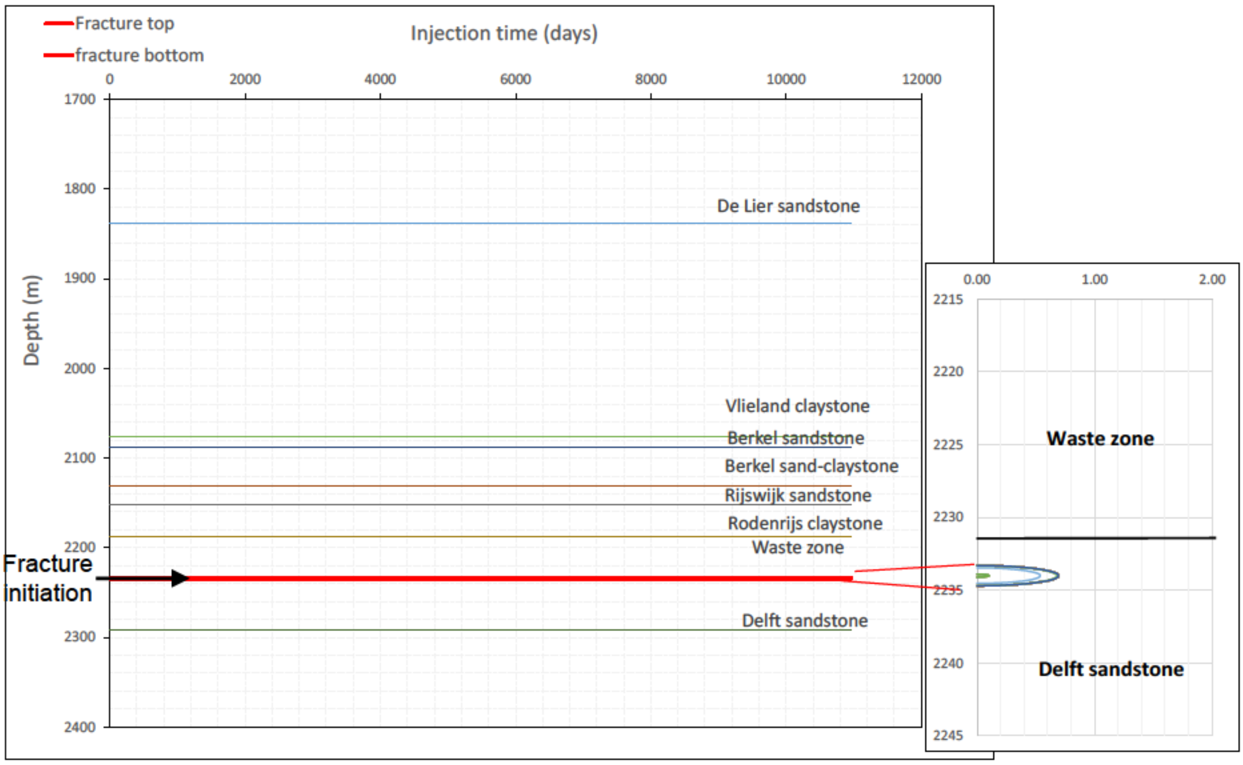

Figure 6-10: Fracture top and bottom as a function of time for base case; fracture contours for sensitivity 3.

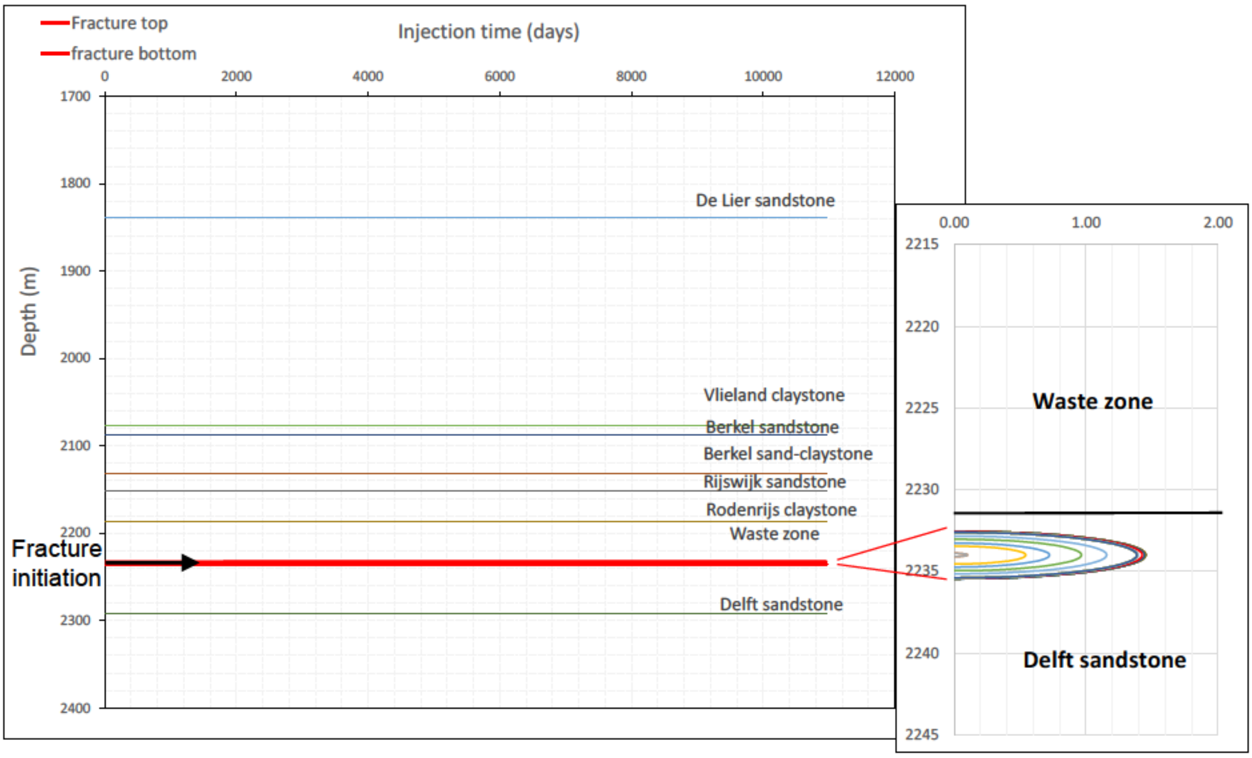

Figure 6-11: Fracture top and bottom as a function of time for base case; fracture contours for sensitivity 4.

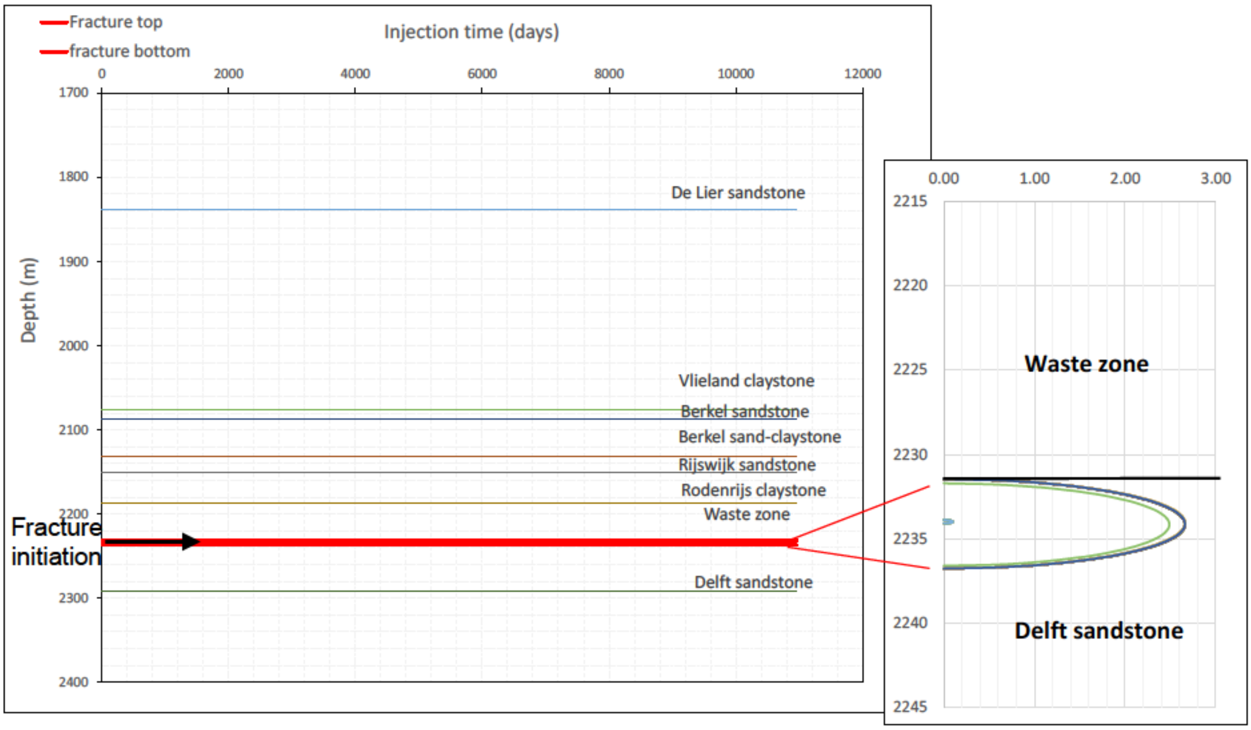

Figure 6-12: Fracture top and bottom as a function of time for base case; fracture contours for sensitivity 5.

7 Conclusions

Reservoir simulations show that in Trias Westland, injection is expected to be possible under matrix conditions for the target injection rates, whilst adhering to the SodM guidelines for maximum injection pressure. This is because the target formation (Delft) has a good k*h.
In order to capture possible “low” cases (e.g. low formation permeability), induced fracture simulations were carried out to estimate the size and (lack of) containment of induced fractures. These simulations show that for all sensitivities, fractures remain small (< 10 m), with only a few meter upwards penetration into the waste zone overlying the Delft formation.
In order to inject safely in the Delft it is advised not to exceed a bottom hole pressure gradient of 0.158 bar/m based on the different fracture simulation scenario’s. The overall risk of loss of containment by induced fracture growth is considered very low for Trias Westland.

8 References

1. Van den Hoek, P.J., 2005. Dimensions and Degree of Containment of Waterflood-Induced Fractures from Pressure Transient Analysis. SPE Reservoir Evaluation and Engineering Journal, October, 377-387.
2. Van den Hoek, P.J., 2017. A Simple Unified Pressure Transient Analysis Method for Fractured Waterflood Injectors and Minifracs in Hydraulic Fracture Stimulation. SPE Productions and Operations Journal, February 2017, 1-17.
3. Stevens, D.G. and Murray, L.R. Predicting Multiple Thermal Fractures in Horizontal Injection Wells; Coupling of a Wellbore and a Reservoir Simulator, SPE 59354 (2000)
4. Svendson, A.P., Wright, M.S., Clifford, P.J., and Berry, P.J. Thermally induced fracturing of water injectors. 1991. SPEPE November 1991, 384-390.
5. Perkins and Gonzalez, 1985. The effect of thermoelastic stresses on injection well fracturing, SPEJ February p. 78-88.
6. Koning, E.J.L., 1988. Waterflooding under fracturing conditions, Ph.D. Thesis, Technical University of Delft.
7. Santarelli, F.J., Havmoeller, O., and Naumann M. 2008. Geomechanical aspects of 15 years water injection on a field complex: an analysis of the past to plan the future. SPE 112944.
8. Gheissary, G. et al. 1998. Simulation of Fractures Induced by Produced Water Re-Injection in a Multi-Layer Reservoir. SPE 54735, presented at the SPE/ISRM Eurock held in Trondheim, Norway, 8–10 July
9. Van den Hoek, P.J., et al. 1999. Simulation of Produced Water Injection Under Fracturing Conditions, SPE Prod. & Facilities 14 (3) August, p. 166-176.
10. Veldkamp, J.G. et al. 2016. Thermal fracturing due to low injection temperatures in geothermal doublets. TNO Report 2015 R11739.
11. De Jager, M. A., Doyle, M.A., Graham, P.J. and Mabillard, J.E. Hydrocarbon habitat of the West Netherlands basin, in Geology of gas and oil under the Netherlands, H. E. Rondeel, D. A. J. Batjes and W. H. Nieuwenhuijs, Eds., Dordrecht, Kluwer Academic Publishers, 1996, pp. 191-210.
12. Den Hartog Jager, D.V., 1996. Fluviomarine sequences in the Lower Cretaceous of the West Netherlands basin: correlation and seismic expression. In: Geology of Gas and Oil under the Netherlands. Kluwer (Dordrecht): Rondeel, H.E., Batjes, D.A.J. & Niewenhuis, W.H. (eds), pp. 229-242.

Appendix A - Short description plus validation of fracture simulator

A.1 Description of fractured water injection model

The purpose of this computer program is to provide via simulation an estimate of lateral and vertical extension of waterflood-induced fractures (both for clean water and produced water injection), of vertical fracture (non-)confinement to target injection zones, of well injectivity, and of the shape and extent of flooded zones. It was developed by merging [1] existing fracturing/CRI [2] and waterflooding [3] software packages during the late nineties of last century into a combined model suited to simulate both hydraulic fracturing (HF), Cuttings Re-Injection (CRI) and Water Injection (WI).

Applications of this program throughout the years have been mainly in the arena of water injection for waterflooding, for reservoir voidage replacement and for (contaminated) water disposal [4-20]. In most of these applications, water injection simulations were carried out to assess issues around fracture containment, sweep and injectivity.

In many waterfloods, fractured water injectors are a common feature. Unintended fracturing in water injectors may occur owing to thermal effects (particularly in offshore areas) or due to pore plugging by impurities in the injection water. Intentional fracturing may be an integral part of the field development plan, since the increased injection potential may enable a significant reduction in the number of injector wells drilled. Furthermore, as a result of fracturing, water purity requirements may be relaxed providing a significant reduction in facilities costs, especially offshore. However, once fracture lengths reach a significant fraction of the well spacing they can have a significant influence on sweep efficiency. Furthermore, if the fracture does not extend over the full height of the formation, non-uniform sweep in the vertical sense may be encountered which may alter field development plans. Finally, intended or unintended fracturing may lead to out-of-zone growth, particularly when injection rates significantly exceed leakoff rates owing to low formation permeabilities and/or limited disposal storage capacity of the target injection zones. Therefore, the accurate prediction of fracture length and height is required.

Our WI/CRI injection model computes fracture dimensions, well injectivities, and flood front displacements for water injection under induced fracturing conditions. This applies both to produced water injection and to clean (e.g. sea-)water injection.

The main shortcoming of the simulator is that it uses an assumed fracture shape (planar vertical fracture consisting of two vertical half-ellipses). Thus, a horizontally symmetric fracture around the injection point is assumed. This can be a limitation in case of strong reservoir asymmetries around the injector (e.g. strong layer tilts). Also, complicated (e.g. 'donut') fracture shapes resulting from strongly differing layer properties (e.g. horizontal stress, Young's modulus) cannot be adequately modeled. Finally, tilted ad/or non-planar (curved) fractures cannot be modeled. In practice, the above shortcomings have turned out to be of limited consequence (i.e. limited with respect to geological and parameter uncertainties), as was shown by many validations. A number of these validations are presented below as examples.

A.2 Validations

A.2.1. Validations against other simulators

Extensive validation [2] was carried out of our fractured WI/CRI model against a number of published results of other fracture simulators, both with a gridded fracture shape [BEM model, 21] and with fixed shapes [22-25]. These validations were carried out on the SPE benchmark set for hydraulic fracture simulators which consisted of 17 cases (called A-O, II and VI) covering contained and uncontained fracture growth (with and without gradient), low and 'high' leak-off, and Newtonian / non-Newtonian injection fluids. Results obtained were overall close to results obtained by the other models and well within the spread of the results [2]. Additional validations were carried out using the well-known HF stimulation field case of SFE-3 that was executed by the US Gas Research Institute in the early nineties [2].

For cuttings re-injection (CRI) applications the capability to simulate 'uncontained' hydraulic fracture growth is essential. Therefore, we also did benchmarks against other models for the situations of uncontained growth in the presence of an in-situ stress gradient, with or without a 'negative' stress contrast (i.e. growth from a higher stress into a lower stress zone).

An example of CRI is shown in Fig. 1 (Northern North Sea, UK sector) [2]. Clearly, our fractured WI/CRI model and the BEM model used in this study yield the highest degree of uncontained upward fracture growth. The other models show far less upward growth. This is a general shortcoming of many of the commercial hydraulic fracture simulation models, which were mostly designed for typical US-hydraulic fracture stimulation settings (strongly contained hydraulic fractures).

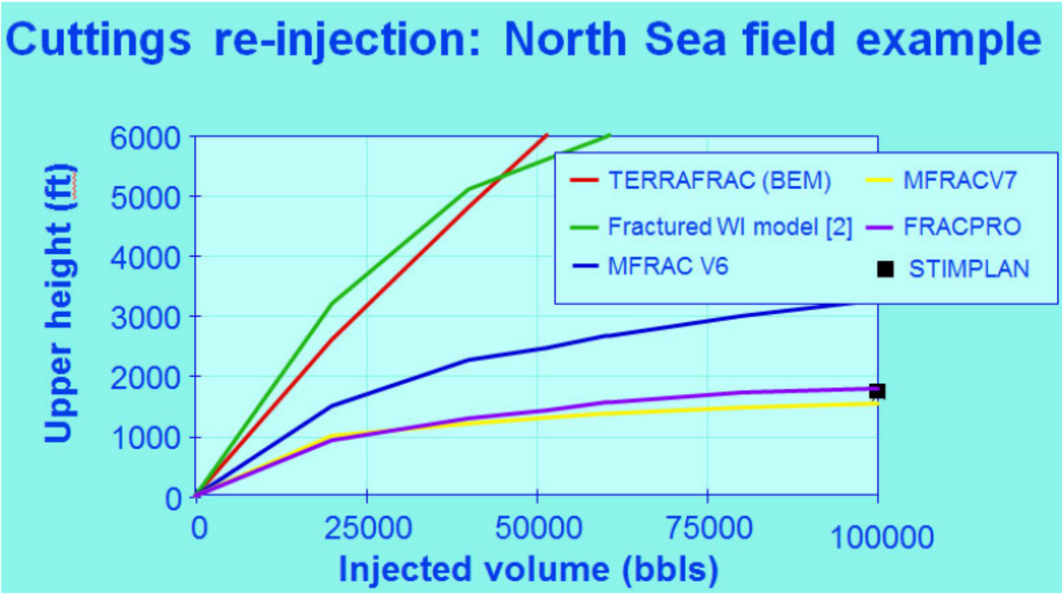

Figure 1. Comparison of different fracture simulators for CRI field example in the North Sea

An example for hydraulic fracture growth in the presence of negative stress contrasts is shown in figure 2 below. As can be seen on the left, the BEM model predicts a fracture with lengthwise 'bulging' in the lower stress zones whilst our fractured WI/CRI model has a fixed shape of two half-ellipses that more or less (on average) follow the contours of the BEM model. In the case on the right, the BEM model also predicts an elliptically shaped fracture, because in this case the impact of the negative stress contrasts is lower as a result of the high net pressure.

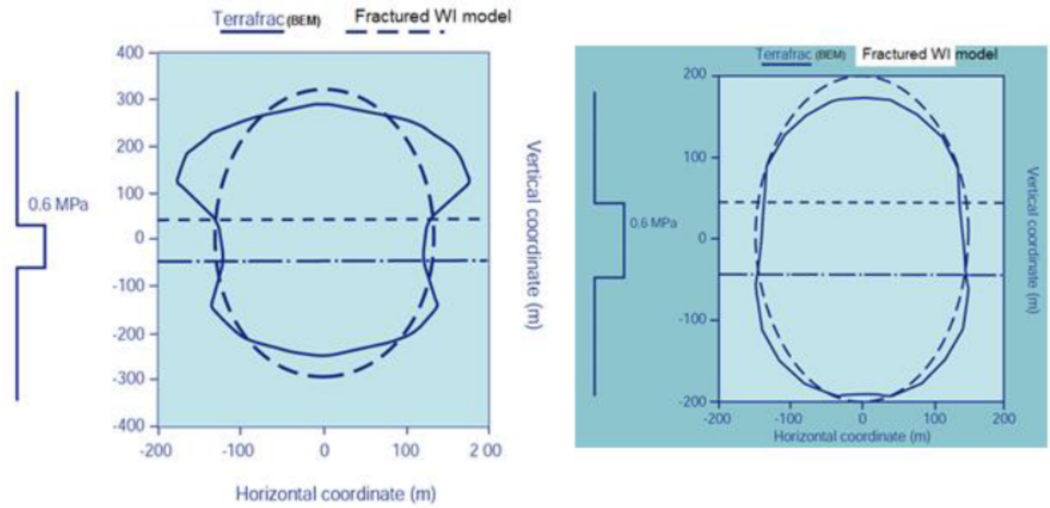

Figure 2. Hydraulic fracture growth from a higher stress zone into a lower stress zone, in the presence of low (left) and high (right) net pressures.

Finally, figure 3 shows the comparisons for a massive hydraulic fracture (MHF) treatment for the NAM offshore the Netherlands [2]. In this case, modeling was required in order to determine the optimum injection depth, and subsequently compute the optimized pump (proppant schedule).

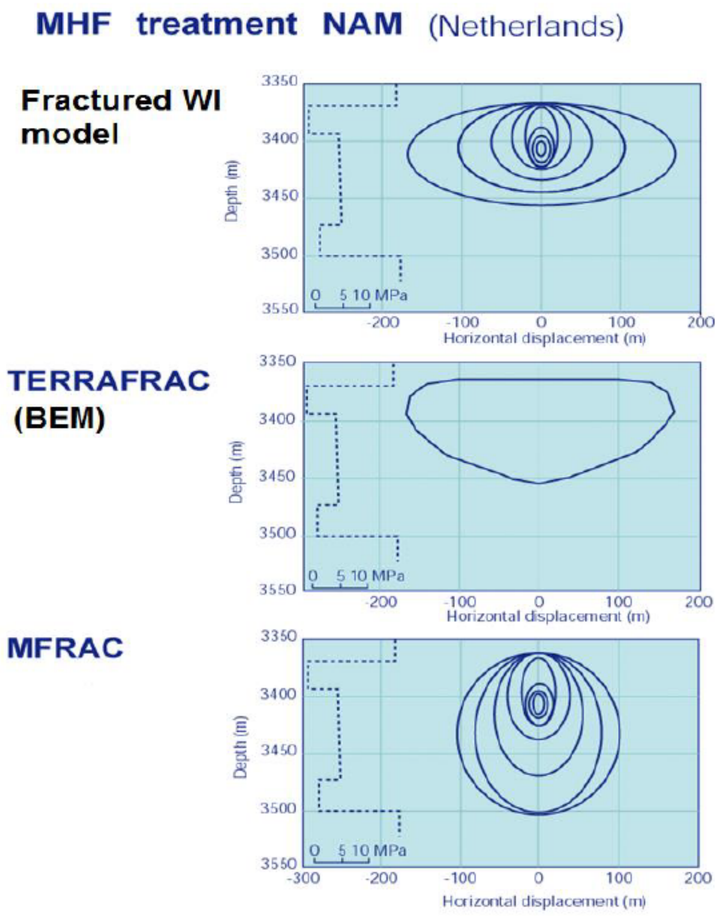

Figure 3: Comparison of WI/CRI fracture model with TERRAFRAC (BEM) and MFRAC for NAM offshore MHF.

A.2.2. Validations against field observations

Our fractured WI/CRI model has been applied to numerous field cases, especially for waterflooding and water injection disposal purposes. Comparison with field observations was always indirectly, e.g. by successful pump schedules based on HF designs [e.g. 2, see above], PLT's in water injectors [5], pressure transient testing [e.g.12-16], fracture breakthrough (or the absence thereof) in nearby producers (waterflooding) [12], in-well tiltmeter measurements [14], temperature logging [16, 19, 20], and continuous monitoring plus history matching of observed injection rates and pressures.

A.2.2.1. Pattern waterflood in Oman: Field development [12]

A pattern waterflood was designed with the intent to inject highly contaminated production water into an oil reservoir with a fairly low reservoir fluid mobility. For such situations, pattern floods with close well spacing are ideally suited to optimize recovery. However, at the same time reasonable injection rates are only achievable when some degree of induced fracturing around the injector is allowed. Obviously this obliges the operator to consider an optimal operational scheme such that on one hand he profits from good injectivity whilst on the other hand, the induced fractures do not grow excessively large, either into the overlying reservoir caprock or into adjacent producer wells.

In order to gain experience with induced fracturing and use this to aid in an optimum field development program, a trial with a five-spot pattern flood was carried out. The layout is shown in figure 4 below.

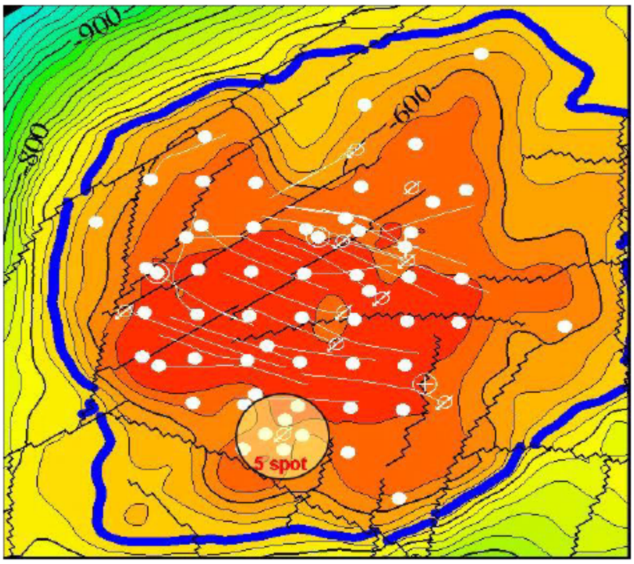

Figure 4: Sub-surface map of reservoir highlighting the area of 5-spot inverted pilot in the south of the field [12].

The pilot was carried out as a step-rate test with long-duration steps in order to also observe the impact on production in neighboring producers. The plot in figure 5 shows the injection rate and duration of each step, and also the computed fracture length by our WI/CRI simulator (coupled to a reservoir simulator [15] to capture the impact on the production rates of nearby wells). As can be seen, for low injection rate (below ca 150-200 m3/d), no appreciable fractures are formed. However, as soon as one exceeds the 200 m3/d, fractures grow with lengths that "rapidly" increase with increasing injection rate. At 400 m3/d injection rate, water breakthrough was seen in adjacent producers. This is in line with the simulations in the sense that the computed fracture length (150-200 m) becomes equal to the well spacing.

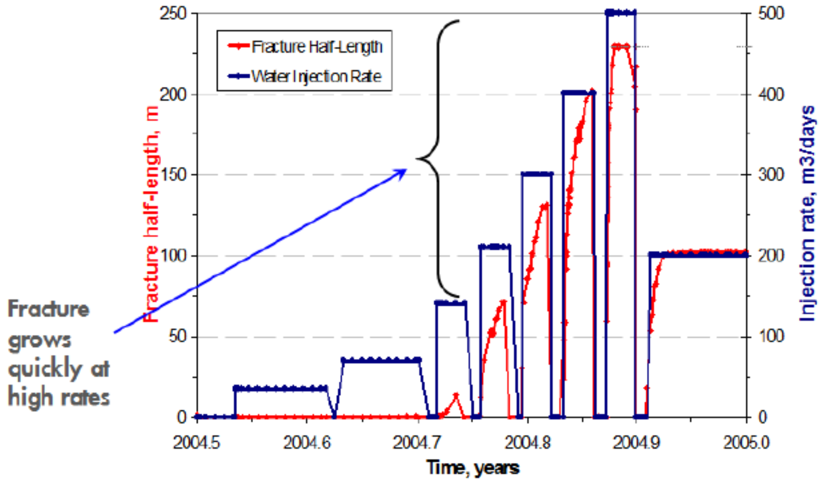

Figure 5: Injection scheme during 5-spot trial plus computed fracture lengths

An important implication of this study was that the size of induced fractures could be kept in check by properly managing the injection rates over the field life. Particularly, it turned out that initially when the reservoir is filled with low-mobility oil, injection rates should be kept at a fairly low level. When gradually increasingly more oil is replaced by higher mobility (injected) water, higher injection rates can be applied without the risk of excessive fracturing.

A.2.2.2. Pattern waterflood onshore Russia (West Siberia): Pattern infill [16]

In this field, a pattern waterflood using low-quality injection water in a light oil field had been already ongoing for some time. The issue at stake here was that pattern infill drill campaigns were being planned and the question was how to manage the induced fractures by an appropriate choice of injection water quality and injection rate, see figure 6.

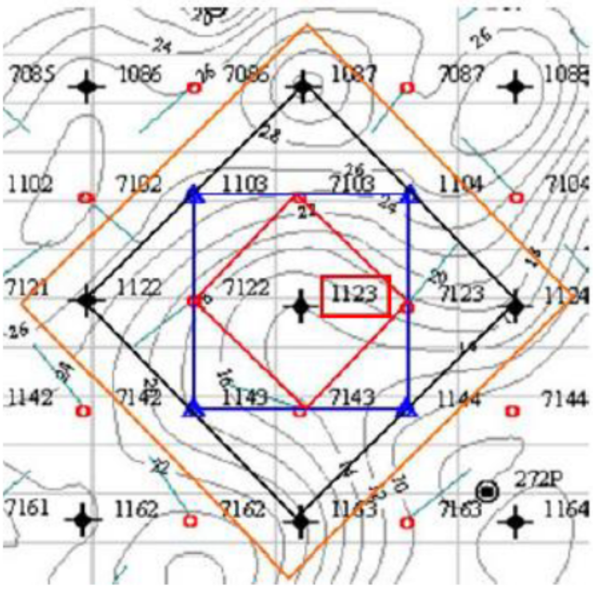

Figure 6: Pattern waterflood lay-out for field in Russia

In this case, fracture dimensions around the injector (no 1123) were monitored on a regular basis by means of pressure fall-off testing (→ fracture length, height) and temperature logging (fracture height). Examples of these measurements are shown in figures 7 and 8 below.

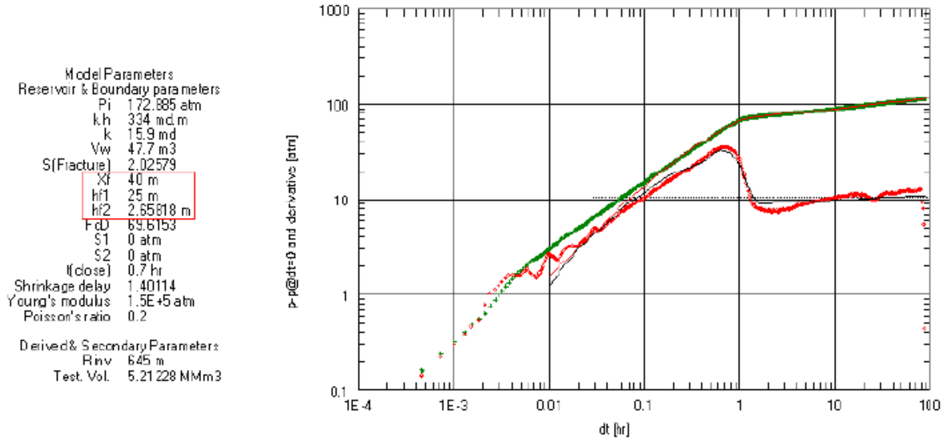

Figure 7: Example of pressure fall-off test and its interpretation

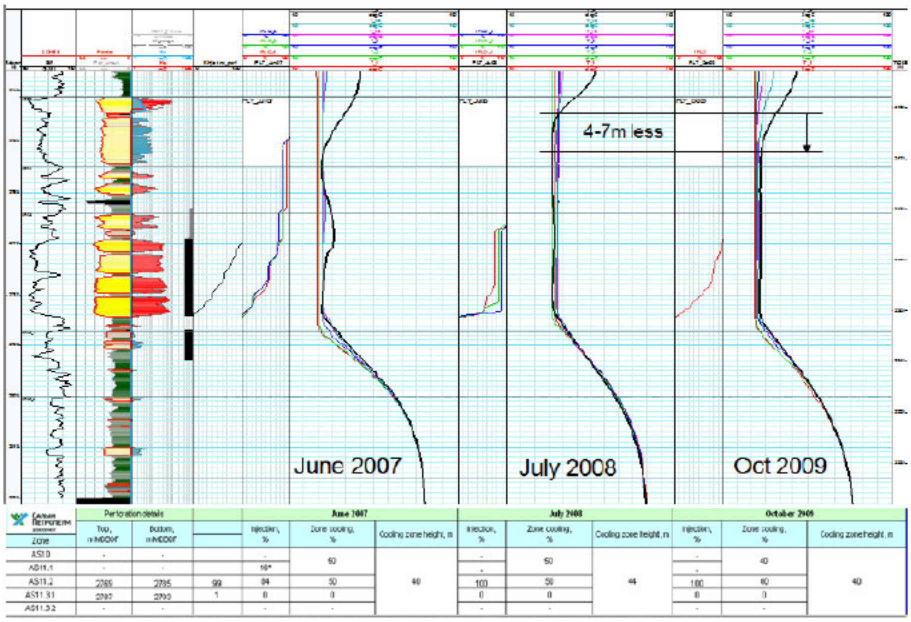

Figure 8: Examples of temperature logs over time and their interpretation

The plot in figure 9 shows the computed fracture length and height by our WI/CRI simulator, in comparison with the fracture lengths as interpreted from pressure fall-off tests. Agreement is reasonable (especially in view of the large data uncertainty), although it appears that the WI/CRI simulator is somewhat on the conservative side at later times.

The results as shown (plus many sensitivities) formed the basis for a decision on infill drilling (pattern, spacing), future injection rate and injection water quality.

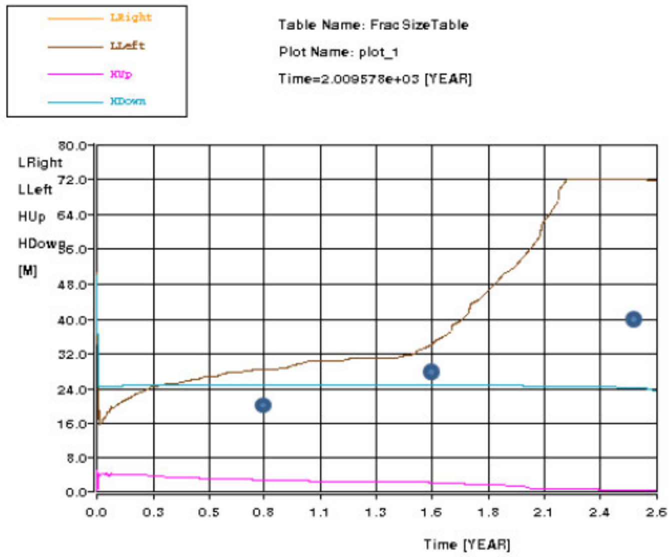

Figure 9. Fracture length growth map of historical injection results: computed versus interpreted from pressure fall-off tests.

A.2.2.3. Large-scale produced water disposal (Oman): Risk of fracture containment [5,14]

Very large-scale produced water injection disposal was pioneered in the late nineties [5]. High volumes of contaminated production water had to be re-injected. A suitable injection horizon was found. However, there was a non-negligible risk that the induced fractures would grow through the overlying caprock shale into potable water-bearing shallow formations.

The basic lay-out is shown in figure 11. Unfiltered produced water is injected into the far flank of the deep formation. This is a fairly homogeneous, medium-permeability (approx. 300mD), medium-strength sandstone with a thickness of several hundreds of meters. The caprock (8 – 18m thick) at approx. 1000 m TVD, provides a sealing shale layer with extensive lateral extent. The carbonate formation above the shale layer is in contact with shallow aquifers, so it is essential that injected production water does not penetrate upwards through the caprock shale. As indicated in the figure, this requirement had an impact on the optimum injection depth.

Figure 10 shows the history-matched injection rates and pressures using the fractured WI/CRI-model, whilst the computed induced fracture is shown in Fig. 11. Its is clear from this figure that the initially planned injection depth was inappropriate. Based on this study, the injection depths for all planned water injection disposal wells were moved down by about 300 m.

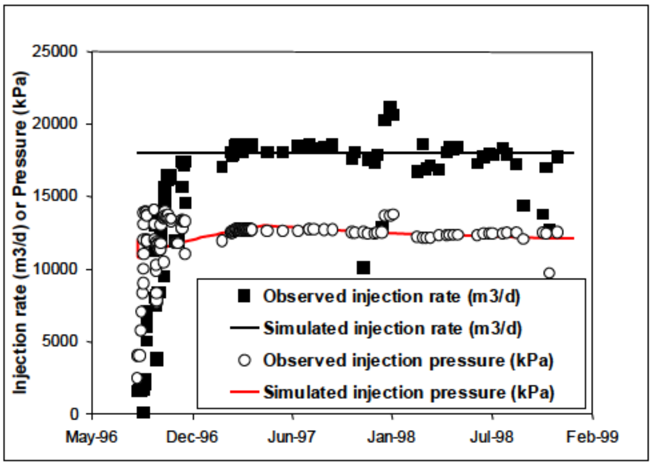

Fig. 10 – Observed and simulated historical injection performance for one of the pilot wells.

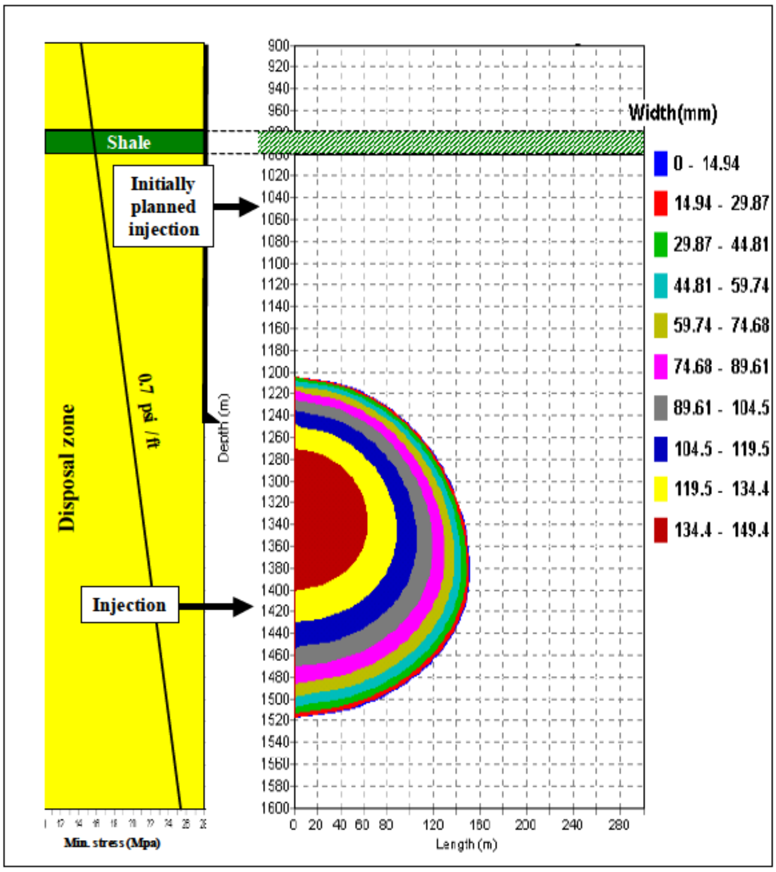

Fig. 11 – Overview of subsurface injection disposal horizons. Also indicated are casing shoe and induced fracture after 20 years of injection for one of the injectors [5].

After the injection disposal wells were on-stream, a number of different surveillance techniques was tried to validate / calibrate the fracture simulations (especially with respect to upward fracture height), but the initial results were fairly inconclusive [5]. Early 2007, the technique of downhole tiltmeters was successfully applied in a trial to measure induced fracture height. This technique has been well-proven for propped fracture applications in tight rocks but applications in medium- to high-permeability waterflood applications had been limited. Because none of the disposal wells had nearby observation wells, it was decided to use the technique of “treatment well tilt” in which the tiltmeters are deployed in the injection well itself. This allows for “optimal” measurement of fracture height (maximum tilt signal), although fracture length cannot be measured in this way. The tiltmeter measurements were combined with pressure fall-off tests after each injection cycle to interpret fracture lengths.

Figure 12 shows the injection / shut-in sequence during the tiltmeter trial. From the horizontal scale of this graph it can be seen that the well had already been injecting ca 4 years prior to the trial. Figure 13 shows an example of a raw tiltmeter signal alongside an "ideal" signal for the case of one planar vertical fracture. As can be seen, ideally the locations of fracture top and bottom are identified from the maxima in the tilt signal, but in our case four (instead of two) of such maxima were observed, leading to some ambiguity in the interpretation of fracture height. In the interpreted results we took this into account by indicating a range for fracture height rather than one value. Finally, Figure 14 shows an example of one of the injection fall-off test results. These results show a pronounced storage-dominated flow period, which is indicative of a large induced fracture [25].

Figure 15 shows a summary of the interpreted fracture heights and lengths from tiltmeter and fall-off tests, together with the fracture dimensions as computed by our WI/CRI fracture simulator, for 4 years injection history, plus the injection cycles as depicted in Fig 12. During the latter of these injection cycles, no reliable tiltmeter signals could be obtained owing to their detachment from the borehole wall (casing). As can be seen from Fig. 15, the computed and measured results are in fairly good agreement, especially when considering the large uncertainties both in the measurements and computations.

Fig. 15 also shows that the maximum total fracture height during the injection trial is far less than the 300 m that was based on earlier simulations (see discussion above, and figure 11). However, this turned out to be mainly the result of two essential differences between the trial on one hand and continuous injection on the other hand: (1) During continuous injection, rates of ca 20,000 m3/d are applied, which was never achieved during the trial, and (2) the limited duration of the trial resulted in induced fractures which were still growing under the influence of transient pressure build-up in the reservoir. Without these two effects, induced fractures are likely to grow towards ca 300 m height, as is illustrated in Fig. 16 which shows the computed result of continuous injection for 4 years at 20,000 m3/d.

Summarizing the above discussion, the simulated sizes of the induced fracture were confirmed by surveillance data (tiltmeter, fall-off), endorsing the policy of perforating water disposal wells at least 300m below the caprock.

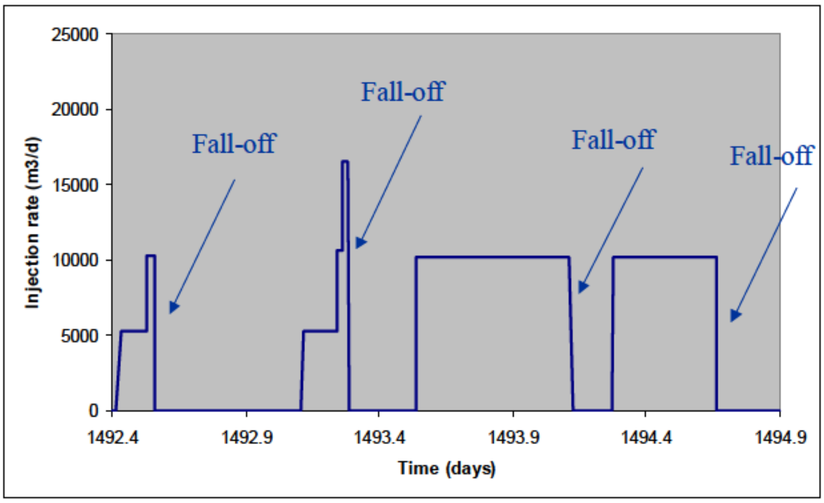

Fig. 12. Oman water disposal well: Injection cycles of tiltmeter test.

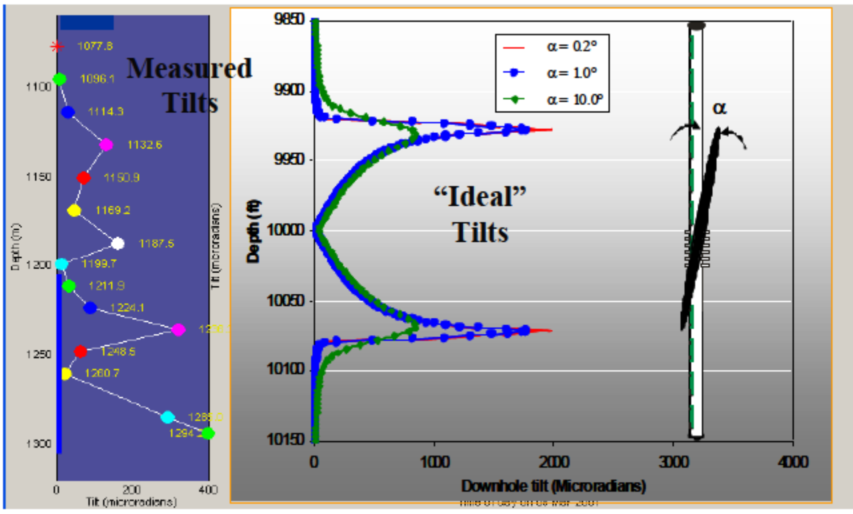

Fig. 13. Oman water disposal well: Example of tiltmeter data.

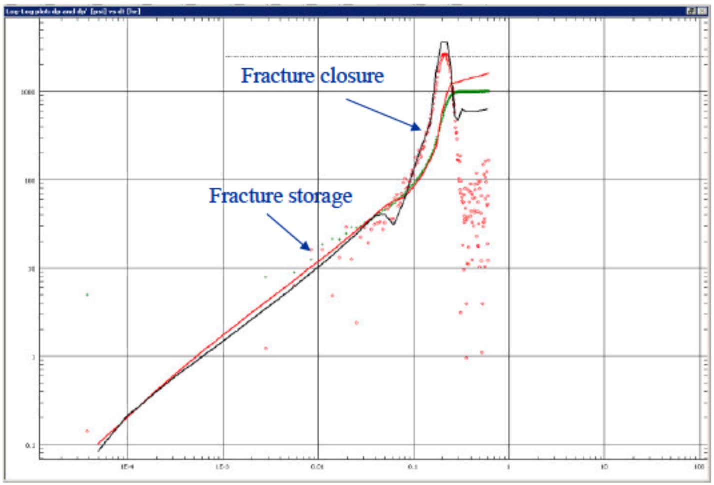

Fig. 14. Oman water disposal well: Example of pressure fall-off test data.

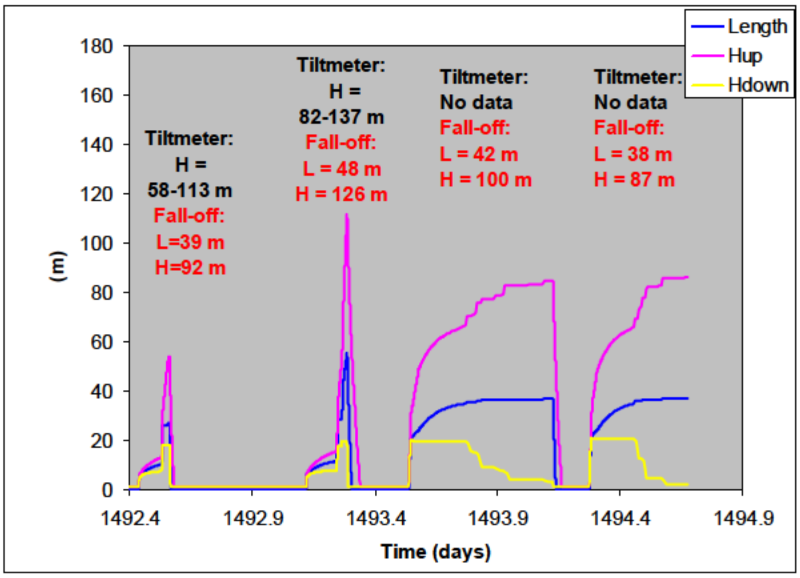

Fig. 15. Oman water disposal well: Summary of tiltmeter test results. Colored curves represent computed results: Length (L), Hup (=upward fracture height), and Hdown (downwards fracture height). H=total fracture height = Hup+Hdown.

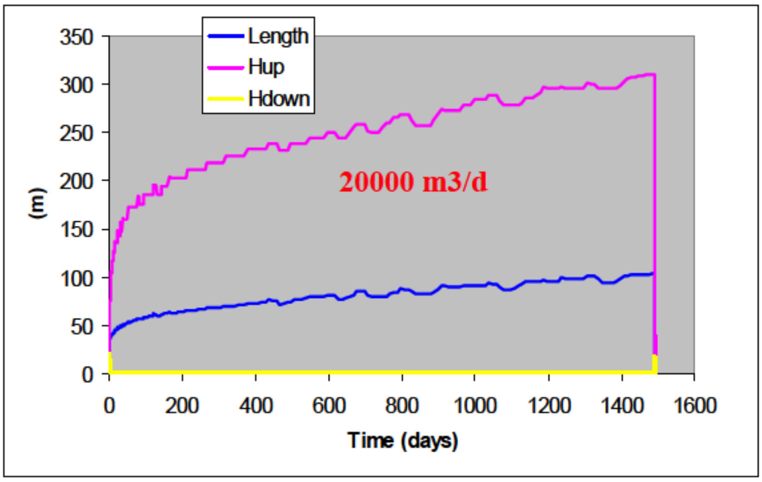

Fig. 16. Oman water disposal well: Computed fracture dimensions for high-rate disposal injection.

A.2.3. Conclusions from validations.

The above paragraphs have illustrated a number of cases where the performance of our WI/CRI fracture simulator was validated both against other simulators and against field data. Overall, the agreement is acceptable, especially in view of the large input data uncertainties for field cases.

There are a number of important points that one has to bear in mind when using this model (or other models with similar functionality) for field applications. First, because of limited data and limited understanding of the subsurface, simulation results can vary widely. Therefore, regular surveillance / monitoring will always be a requirement. Such surveillance results can be history-matched and subsequently used to update the input data. Secondly, it is vital that the user has a proper qualitative 'physical' understanding of the results from a simulator – i.e. there should be no using hydraulic fracture simulators in 'black box' mode. Trying to understand the results from hydraulic fracture simulators can often be quite challenging, but it does help to track deficiencies in the input data, in the understanding of the subsurface, and/or the hydraulic fracture simulator itself.

REFERENCES

1. G.Gheissary, P.A. Fokker, P.J.P. Egberts, F.J.T. Floris, G. Sommerauer and C.J. Kenter. Simulation of Fractures Induced by Produced Water Re-Injection in a Multi-Layer Reservoir. SPE 54735, presented at the SPE/ISRM Eurock '98 held in Trondheim, Norway, 8–10 July 1998.
2. P.J. van den Hoek. New 3D model for optimised design of hydraulic fractures and simulation of drill cuttings re-injection. SPE 26679, presented at SPE Offshore Europe, Aberdeen (1993).
3. Koning, E.J.L., Waterflooding under fracturing conditions, Ph.D. Thesis, Technical University of Delft, 1988.
4. Van den Hoek, P.J., Matsuura, T., De Kroon, M., and Gheissary, G.: "Simulation of Produced Water Injection Under Fracturing Conditions", SPE Prod. & Facilities 14 (3) August 1999, p. 166-176.
5. P.J. van den Hoek, G. Sommerauer, L. Nnabuihe, and D. Munro. Large-scale produced water re-injection under fracturing conditions in Oman. SPE 87267 (ADIPEC 0963), presented at Abu Dhabi Petr. Conference (2000).
6. P.J. van den Hoek, Z.I. Khatib, and G.J. Siemers. Causes of Injectivity Problems During Fractured Water Disposal and Their Remediation. SPE 74416, presented at SPE IPCEM, Villahermosa (2002).

7. M. Bai, S. Green, and P.J. van den Hoek. A parametric analysis of deep injection for waste disposal using a 3-D hydraulic fracture simulator (presented at NARMS conference, Toronto, 2002).
8. J.C. Noirot, P.J. van den Hoek, Dirk Zwarts, Hans Petter Bjoerndal, SPE, Rik Drenth, R. Al Masfry, B. Wassing, J. Saeby, M. Masoori, and A. Zarafi. Water Injection and Water Flooding Under Fracturing Conditions. SPE 81462, presented at SPE MEOS, Bahrain (2003).
9. S. Sathyamoorthy, P. Priyandoko, K.B. Flatval, A. Bulang, P.J. van den Hoek, and Y. Qiu. Radical Approach to Water Injection Scheme for Barton. SPE 84885, presented at SPE improved oil recovery conference in Asia Pacific, Kuala Lumpur (2003).
10. K.I. Ojukwu and P.J. van den Hoek. A New Way to Diagnose Injectivity Decline During Fractured Water Injection By Modifying Conventional Hall Analysis. SPE 89376, presented at SPE/DOE conference on improved oil recovery, Tulsa (2004).
11. B. Hustedt, Y. Qiu, D. Zwarts, and P.J. van den Hoek. Modeling Water-Injection Induced Fractures in Reservoir Simulation. SPE 95726, presented at SPE ATCE, Dallas (2005).
12. J. Sæby, H.P. Bjørndal, and P.J. van den Hoek. Managed Induced Fracturing Improves Waterflood Performance in South Oman. IPTC-10843, presented at IPTC, Doha (2005).
13. Hustedt, B., Qiu, Y., Zwarts, D., van Schijndel, L., and P.J. van den Hoek. The Impact of Water-Injection Induced Fractures on Reservoir Flow Dynamics: First Applications of a New Simulation Strategy. IPTC-10689, presented at IPTC, Doha (2005).
14. P.J. van den Hoek, B. Hustedt, M. Sobera, H. Mahani, R.A. Masfry, J. Snippe and D. Zwarts. Dynamic Induced Fractures in Waterfloods and EOR, SPE 115204, presented at the 2008 SPE Russian Oil & Gas Technical Conference and Exhibition held in Moscow, Russia, 28–30 October 2008.
15. B. Hustedt, D. Zwarts, H.-P. Bjoerndal, R. Masfry, and P.J. van den Hoek. Induced Fracturing in Reservoir Simulations: Application of a New Coupled Simulator to Waterflooding Field Examples. SPE Reservoir Evaluation & Engineering Journal, Vol. 11 (June 2008), p. 569-576.
16. A. Aniskin, I. Chmuzh, R. Sakhibgareev. Waterflood induced fracturing in the West Salym field. SPE 136560, presented at the 210 SPE Russian Oil & Gas Technical Conference and Exhibition held in Moscow, Russia, 26-28 October 2010.
17. Van den Hoek, P.J., Al-Masfry, R., Zwarts,D., Jansen, J.D., Hustedt,B., and Van Schijndel, L. Waterflooding Under Dynamic Induced Fractures: Reservoir Management and Optimization of Fractured Waterfloods. SPE Reservoir Evaluation & Engineering Journal, October 2009, p.671-682.
18. M. Khodaverdian, T.G. Sorop, P.J. van den Hoek, S.Sathyamoorthy and E. Okoh. Injectivity and fracturing in unconsolidated sand reservoirs: Waterflooding case study, offshore Nigeria. Paper Arma 10-139, prepared for presentation at the 44th US Rock mechanics Symposium and 5th US-Canada Rock mechanics Symposium, Salt Lake City, June 27-30, 2010.
19. M. Zwaan, R. Hartmans, S. Schoofs, B.R. de Zwart, G. Rocco, R. Adawi, F. Saadi, K. Shuaili, J. Lopez, J. Ita, T. L'Homme, T. Sorop, Y. Qiu, P.J. van den Hoek, F. Al-Kindy, S. Busaidi, and J. Fraser. EOR Field Management Through Well-Planned Surveillance. SPE 154620, presented at the SPE EOR Conference at Oil and Gas West Asia, Muscat, Oman, 16-18 April 2012.
20. A. Petrik and P.J. van den Hoek, Multi-zone Waterflood Top Seal Integrity Assurance: insights from advanced Pressure Fall Off analysis using Smart Well and DTS technologies offshore Sakhalin, Russia. SPE-181985, presented at the SPE Russian Petroleum Technology Conference and Exhibition held in Moscow, Russia, 24–26 October 2016.
21. Dougherty, R.L. & Abou-Sayed, A.S., Evaluation of the influence of in-situ reservoir conditions on the geometry of hydraulic fractures using a 3D simulator. SPE 13275 (1984).

22. Meyer, B.R., Three-dimensional hydraulic fracturing simulation on personal computers: Theory and comparison studies. SPE 19239 (1989).
23. Advani, S.H., Khattab, H. & Lee, J.K., Hydraulic fracture geometry modelling predictions and compartisons. SPE 13863 (1985).
24. Bouteca, M.J., Hydraulic fracturing model based on a 3-D closed form: tests, analysis of fracture geometry and containment. J. SPEPE, November 1988, p. 445.
25. Cleary, M.P., Barr, D.T. & Willis, R.M., Enhancement of real-time hydraulic fracturing models with full 3-D simulation. SPE 17713 (1988).
26. Van den Hoek, P.J. Dimensions and Degree of Containment of Waterflood-Induced Fractures from Pressure Transient Analysis, SPERE, October 2005, 377-387.